Bachelor Thesis

# Synthesis and characterization of aramid-honeycomb reinforced silica aerogel composite materials

A study of Methyltrimethoxysilane (MTMS) / Tetraethyl orthosilicate (TEOS) based silica-aerogel composites prepared by a two-step sol-gel process and supercritical drying

**October 2014**


**Matthias Rößler**
Matriculation Number: 305853

**Abstractor:** Prof. Dr. Dr. h.c. L. Ratke
Prof. Dr. S. Reh
**Supervisor:** Dr. B. Milow
Dipl.-Ing. M. Schwan


DLR

RWTH AACHEN UNIVERSITY

## Declaration

I hereby declare that I have made the following bachelor thesis independently. To create this work, the in the source directory specified aids were used. Passages which were taken verbatim or in substance from published or unpublished sources are marked as such.

Matthias Rößer, Aachen den 24.10.2014

# Synthesis and characterization of aramid-honeycomb reinforced silica aerogel composite materials

A study of Methyltrimethoxysilane (MTMS) / Tetraethyl orthosilicate (TEOS) based silica aerogel & aramid honeycomb prepared by a two-step sol-gel process and supercritical drying

Matthias Rößler*

Institut für Werkstoff-forschung, Deutsches Zentrum für Luft-und Raumfahrt (DLR), 51170 Köln, Germany

**THESIS INFO**

***Contact:***
matthias.roessler@rwth-aachen.de
***Submitted:***
24. October 2014
***Abstractor:***
Prof. Dr. Dr. h.c. Lorenz Ratke
Prof. Dr.-Ing. Stefan Reh
***Supervisor:***
Dr. Barbara Milow
M.Sc. Marina Schwan

***Keywords:***
Aerogel composite material
Honeycomb
MTMS
Nano-porous structures
Silica aerogels
Sol-Gel
Supercritical drying
TEOS
Thermal insulation

**ABSTRACT:**

In this thesis three different nano-porous silica aerogels filled in the pores of aramid honeycomb structures of different dimensions are investigated. The composites have a prospective use as insulation material. They were prepared by employing a two-step acid–base sol–gel process utilizing the silicon alkoxides methyltrimethoxysilane (MTMS) or tetraethylorthosilicate (TEOS) as precursors and supercritically dried in $CO_2$. In order to drastically improve the mechanical properties of silica aerogel monoliths, different aerogel formulae were synthesized in aramid honeycomb structures of different height and cell size. Each recipe, called super-flexible SA1, semi-flexible SA2 and inflexible SA3, could be synthesized in the honeycomb pore space. For the first two composites, based on super-flexible SA1 and semi-flexible SA2, suitable interface bonding and thermal conductivities of 0.036-0.041 W/mK and 0.0395-0.0455 W/mK could be measured. Honeycomb dominated apparent Young's moduli of up to 0.137 MPa in-plane / 21.13 MPa out-of-plane for SA1 such as 0.16 MPa in-plane / 20.16 MPA out-of-plane for SA2 could be measured. SA3 on the other hand showed such a bad adhesion to the honeycomb, that further testing was not possible. From both the positive and negative results criteria for successful aramid-honeycomb reinforced aerogel composite fabrication were identified: Primarily reducing shrinkage of the aerogels and honeycomb used such as ensuring good adhesion between the two materials. The results confirm the assumption that the aramid honeycombs have a minor effect on the thermal conductivities of the composites (only ~10-15% increase in comparison to the pure aerogels), though the mechanical properties are increased significantly (peak strength and the range of linear elastic behavior represented by the apparent Young's modulus, which increased in magnitude by a factor of more than 1000 for SA1-based composites and of more than 100 for SA2-based composites for out-of-plane compression). Hence it is demonstrated that aerogel-honeycomb composite materials have potential to enable new practical applications for silica aerogel materials via diminishing their limiting fragility.

# Contents

# I. Introduction

The thermal properties of aerogels have been the focus of research since Kistler's first synthesis of aerogels [Aeg1]. Especially the impressive low thermal conductivities of silica aerogels down to 0.01 W/mK [10,22,24] are promising for countless new insulation applications in aeronautics, mobility or the building industry [4]. One factor which hinders the industrial utilization of aerogels is their fragility. Low Young's moduli (for example 0.074 MPa for the semi-flexible silica aerogel used compared to 12-20 MPa of the insulation material Styrofoam [5]) and their characteristic brittleness prevent the usage in many fields of application. Therefore reducing the rigidity and brittleness of aerogels had been one of the key aims of researches at all times. In addition to attempts modifying the microstructure chemically [6], also the idea of aerogel composite materials has been presented by various groups [7-12]. One approach promising significantly increased mechanical properties are honeycomb structures filled with aerogels and therefore would make new insulation applications possible.

This bachelor thesis is about the manufacturing and characterization of aramid-honeycomb reinforced silica aerogel composite materials. Three different aerogels, super-flexible, semi-flexible and stiff, were prepared by a two-step sol-gel process and supercritical drying of MTMS and (TEOS) based gels in aramid honeycombs of different cell sizes and height. The first part of this bachelor thesis deals with theoretical aspects needed for the manufacturing, testing and analysis of the results obtained. Secondly the experimental procedures are described. Finally, the results are listed, discussed and conclusions are drawn.

# II. Theory

## A. Aerogels

### i. Aerogels in general

The name makes it quite evident: Aerogels have something to do with air. Aerogels are versatile ultra-lightweight mesoporous materials which are synthesized by traditional low-temperature sol-gel chemistry in a first step, followed by specialized but well known drying-techniques. This leads to the solid but filigree network of thin ligaments being retained, but then surrounded by air instead of liquid. Due to the fact that the thickness of the ligaments determines the final density and porosity of the aerogel, a low density (~0.003 g/cm$^3$) of only three times that of air can be achieved [13]. This nanostructure is also the reason for a unique combination of many outstanding properties. A lot of different aerogels, from brittle to highly flexible, can be fabricated and are deployable from -200°C to1400°C. From the characteristic chain-like ordering of particles, a hydrophilic or hydrophobic gel structure with a porosity of up to 99.8%, an surface area in the range of 100–2000 m$^2$/g [14], an unmatched high thermal insulation value (down to 0.005 W/mK), an ultra-low dielectric constant (k=1.0-2.0), and a low index of refraction (~1.01 - transparency close to glass) can be synthesized. They can also be electro conductive and flame retarding, but tend to be brittle and fragile with a low shear resistance in most cases [4]. For many thermal, optical, catalytic and chemical applications, which do not require mechanical stability, aerogels are superior, but yet to be adapted candidates. Furthermore, this set of properties can tailored by countless different chemical compositions. This explains the increasing interest and number of publications about aerogels, both in fundamental research and technical applications, which steadily grows since Kistler's first supercritical aerogel synthesis in 1931 [13]. Since 1992 also an ambient pressure drying process for silica aerogels has been available, which can reduce cost significantly. [15]

Since the late 1960s, when application-oriented research and development increased concomitant with the rapid development of the sol-gel process [4], a lot of different aerogels have been synthesized, especially inorganic oxides (silica, titania, alumina), organic resins (melamin-formaldehyde, resorcinol-formaldehyde) and biopolymers (chitosan, cellulose etc.) [16]. A common definition specifies such materials as aerogels, in which the pore liquid of the gel is exchanged with air without damaging the characteristic network structure „too much".

Because shrinkage- and rearrangement is common during the drying of the gel, „too much“ cannot be exactly specified. [13].

The structure of the network and therefore the properties of the aerogel depend greatly on the chemicals used, the synthesis and the subsequent process of drying. Some critical parameters have to be complied with to ensure reproducible results. The aerogels' structures are typically built-up by nano-sized particles from aqueous solution, which form a network of open pores in the nanoscale range. This nanostructure, originating from the gel, is the reason why these ultralow-density materials exhibit interesting properties, such as extreme low thermal conductivity, high inner surfaces or good sound insulation.

When using the sol-gel method for synthesis, at first, a so called sol, consisting of discrete colloid particles, must be transformed to a gel. To do this the so called two step acid-base sol-gel method was used. It is composed of an acid-catalyzed hydrolysis of the silica precursor in the first step, and a condensation reaction under alkaline conditions in the second step. This method was described by Kistler and applied by Nicolaon and Teichner [17]. When a gel network is established, it needs to be strengthened for further. The final properties of the aerogels are strongly influenced by the structure developed during this so called aging, because the chemical reactions that lead to gelation continue long after the sol changes into gel [18]. Since aging leads to a condensation of unreacted monomers and oligomers to the already existing gel backbone and therefore enhances the network, it will reduce the shrinkage in the subsequent drying process [19]. Finally a super-, subcritical or even freeze-drying must follow the gelation and aging in order to remove the remaining pore solvent [13]. After this aerogels are obtained. In supercritical drying, the solvent can be removed from the pores in the supercritical state, because there is no liquid-vapor interface and therefore no capillary pressure occurs. Otherwise the evaporation of solvent from the micropores in the gel would create local differential stresses due to nonuniform pore size distribution, which might lead to the destruction of the network.

In summary, this process is needed for most aerogels to avoid drying shrinkage. Since around 1990, this drying is done with supercritical carbon dioxide as a solvent for gels containing organic solvent, which made the process significantly more economical and safer [4].

In some applications, for example in aerogel-incorporated concrete or in the sands for sandcasting, aerogels can be used as a particulate material. Other applications require more complex bound forms, which cannot be realized with aerogels due to their brittleness. The reason why especially objects purely consisting of aerogel are difficult to handle is their high porosity, which causes a very brittle network. Furthermore, silica-based aerogels tend to release dust on handling [14]. Because most silica-aerogels are hydrophilic and thus OH-groups absorb moisture from humid surroundings with time, some long-term technological applications are not feasible [21]. However, large scale fabrication is expensive when supercritical drying is required, which is the reason why aerogel-based materials tend to compete with other insulation materials only in applications where cost is of lower priority. The ambition to mitigate the fragility and brittleness of aerogels brings up the idea of composite materials, since in particular the improvement of mechanical strength is beneficial for many industrial applications.

Since aerogels have a unique combination of properties, countless applications of silica aerogels have been investigated [22-25]. Only a few ones are listed in Fig.1 [26]. Most attention is paid to aerogels in the fields of application dealing with thermal insulation. Their unmatched low thermal conductivity, paired with extreme low densities, and good acoustic insulation have brought up many ideas of use in automotive and aeronautics such as in the building industry and high temperature isolation of industrial furnaces [26-28]. With increasing environmental responsibility and the need for a more sustainable energy consumption aerogels promise exceptionally potent solutions.

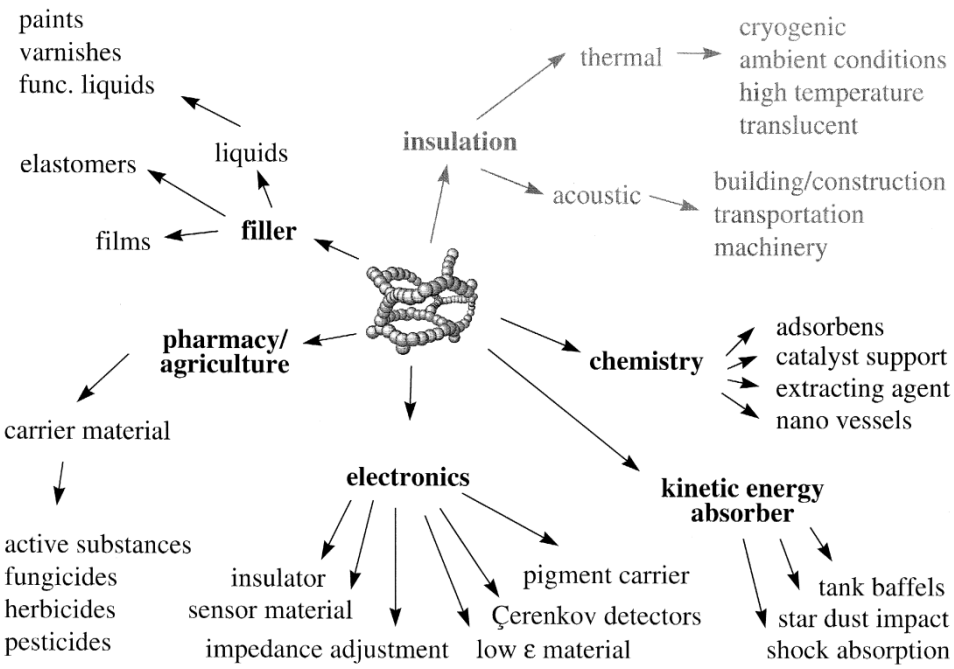


**Fig. 1:** Application fields for aerogel products [26]

### ii. Silica aerogels

Silica aerogels represent well-investigated attractive candidates for many applications [1–16]. Their structure is often described by a remarkable low thermal conductivity around 0.02–0.08 W/mK [2]. They exhibit low bulk densities density of 20–240 kg/m$^3$ [29], high surface areas of up to 1,400 m$^2$/g [29], high optical transmission ~90%, high porosity ~ 99% and a low dielectric constant ≈ 1[1] [31]. Silica aerogels are often composed of molecules like SiOx(OH)y(OR)z, for example of Tetraethylorthosilicat [13]. Their often brittle structure is composed of small spherical silica clusters connected to each other and forming a three-dimensional networks. It is heat-resistant and therefore promises new applications especially in the temperature range of up to 500°C. In recent years, also flexible silica aerogels could be established [14].

[1] The permittivity of transparent materials is determined by the square of the refractive index and therefore silica aerogels have typically a dielectric constant (permittivity) of a bit more than 1.

## B. Honeycombs

### i. General description and properties of aramid honeycomb

Generally, when a light-weight mechanical reinforcement of structures is needed, engineers might think of the well-established honeycomb structure. The commonly columnar and hexagonal cells form a structure of low density but relative high out-of-plane compression and shear properties. Honeycomb is characterized by a high strength-to-weight-ratio but minimized amount of material used and cost at the same time. With the development of the three traditional honeycomb production techniques expansion, corrugation and molding around 1900 [32], honeycomb production experienced impetus in the first decade of the 20th century with first suggestions for applications in aviation by Junkers [33] or Dornier [34]. Today, honeycomb composite structures have proven their merit in numerous engineering and scientific applications.

**Fig. 2:** Profile of a sheet of aramid honeycomb

Aramid honeycombs excel as ultra-lightweight material for structure reinforcement when good thermal and fire retardant are desired. They are predominately used as a core in sandwiched structures to meet design requirements for highly stressed components. Their general properties are listed below in Tab. 1. The combination of phenolic resin and aramid paper results in excellent toughness, strength and chemical resistance (**Fig. 2**).

The most important honeycomb material for this study is Nomex aramid paper. The utilized honeycomb are manufactured from this flame-resistant meta-aramid “Nomex” via the expansion process, which is shown in **Fig. 3**. Sheets of aramid paper, which are formed into a

honeycomb structure, are bonded together and coated with phenolic resin. Further information on the process can be found in [2].

Concerning the manufacturing of aramid honeycomb materials, the honeycombs are characterized by the following properties: All of the aramid honeycombs can be formed by heating to approximately 210°C and cooling while held in the required shape. This allows more complex shapes. They are easily cut and provide a good bonding surface for self-adhesive systems. Unfortunately they tend to absorb moisture and drying the core before bonding is recommended by the producer for maximum performance [35].

Today, a wide variety of materials can be formed into a honeycomb composite. For example porous structural ceramics can be of technological interest owing to their potential for use in applications that require high permeability, a high surface area, and good insulating characteristics. Honeycomb of paperboard on the other hand is utilized in package cushioning due to its low production cost [36].

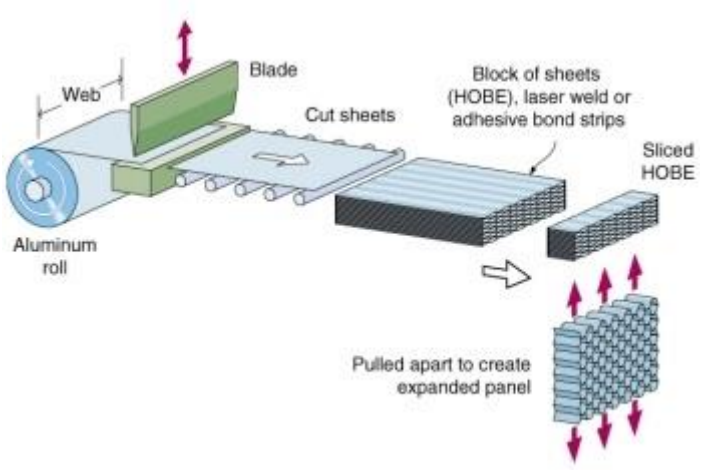


**Fig. 3:** Visualization of the honeycomb production technique „expansion“ [37]

Since the objective of this research is to validate and explore the potential of aerogel-honeycomb-composites as insulation material, standard hexagonal aramid-honeycombs are used. They are the most common cellular honeycomb configuration utilized in industry and easily available from different manufacturers with different properties. Because the honeycomb panels may react differently depending on the orientation of the structure one has to distinguish between the so-called L- and W-direction [Fig. 4]. This behavior is also called orthotropic. A lot of other configurations than the hexagonal are available, for example with

increased “W-” to “L”-shear properties, to further tailor the composites’ properties to their desired application.

**Tab. 1:** Material properties of Nomex honeycombs [Schütz]

| | |
|---|---|
| Mechanical features:<br>• Superior mechanical properties with high strength to weight ratios<br>• High dimensional stability to impact damage, under heat and moisture | Thermal properties:<br>• Low thermal conductivity.<br>• High temperature capabilities, service temperature up to 180°C<br>• Fire retardant and rated as self-extinguishing<br>• Low heat generation, smoke density and low fumes toxicity when tested to FAR 25.853 and ATS 1000. |
| Chemical resistance:<br>• Excellent resistance to corrosive attack by chemicals, with strength reductions of less than 10% following immersion in different fluids (A10) | Electrical properties:<br>• Electrical insulator<br>• Transparent to radio and radar waves |

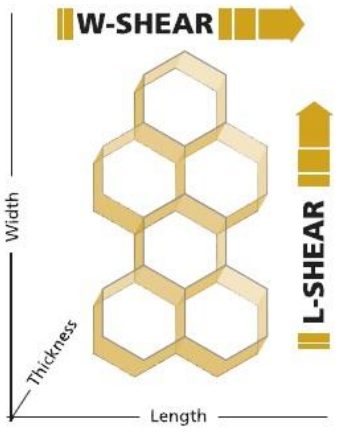


**Fig. 4:** Definition of the width-, length- and thickness direction

### ii. Technical data of the utilized aramid honeycomb

Three different types of hexagonal honeycomb were used: Two variants of the Schütz Industry Services' honeycomb C1, with cell sizes 3,2 mm and 6,2 mm and a density of 29 kg/m³ and 24 kg/m³, such as the Hexweb honeycomb A10-3.2 with 5 mm cell size and 32 kg/m³ density. All of them are rated qualified for aeronautical applications. A tabular listing of all the mechanical properties of the honeycombs used is presented in section III.C). All three variants consist of phenolic resin coated aramid paper, formed in a hexagonal shape in heights from 5-15 millimeter. Two different suppliers were chosen to show that the overall results do not depend on a particular honeycomb. For further experiments, cell sizes from for example 3.2 mm to 9.5 mm with a density range from 24 kg/m$^2$ to 144 kg/m$^2$ are available from Schütz Industry Services [38]. Their specification can be derived from their name, as described in Fig. 5.

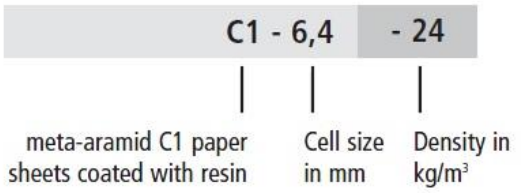


**Fig. 5:** Explanation of naming for Schütz Industry Services' honeycombs C-6.4-24. The position of the specifications cell size and density are switched in the Hexweb nomenclature for A10-3.2 .

Tolerances on the honeycomb specifications are given as follows: Density can be ± 10% of the nominal density, slice thickness may vary ± 0.125mm and manual cutting of samples can result in a ± 5% nominal expanse.

# C. Honeycomb reinforced aerogel composite materials

## i. State of the Art

Composite materials have the appeal that they can combine the properties of each constituent to some extent. Thereby materials with desired properties can be custom-made, which is the reason why they are of high value for engineers. Honeycomb structures in particular are long and well-established in this field, as shown in section II.B). Their properties (being light although having a high mechanical load capacity) come in handy when trying to diminish the aerogels‘ fragility. Especially the low volume fraction, which the honeycomb has in the composite, lends itself to composite insulation materials: The volume fraction of the insulating aerogel remains high in the composite too and will thereby constitute the thermal conductivity of the composite. On the other hand, the aerogel can greatly benefit from the reinforcing honeycomb, as its mechanical stability is magnitudes higher. When good adhesion between the two components can be ensured, honeycomb reinforced aerogel composites sound promising.

For example Sun-Wook Hong et al. proposed porous silica aerogel/honeycomb ceramic composites fabricated by an ultrasound stimulation process. It is pointed out that low shrinkage was a key factor for increasing the interface compatibility with the aerogel/honeycomb ceramic composites, and therefore the success of the combination [39]. Sunil C. Joshi proposed granular silica aerogels to be used as fillers, in carbon or glass composite sandwich structures, with which different insulation applications are imaginable. [40]. Schwan et al. report on a composite consisting of aramid honeycombs filled with novel flexible rubber-like resorcinol-formaldehyde aerogels, which were supercritically dried in CO2 and showed almost no shrinkage [41].

Just these few publications on honeycomb reinforced aerogels can be found, meaning that the field of honeycomb-reinforced or filled aerogels is new. Therefore the investigations presented here try to further explore the field.

## ii. Theoretical calculation of properties in composite materials

To estimate the mechanical properties of composite materials in a simple manner the rule of mixtures can be used. It assumes that the properties of the composite correlate to the properties of each material involved, weighted by their volume fraction. The foundation for this

approach is given by the principles of linear springs. In the given case a parallel circuit or a series connection is assumed for the calculation [42].

If the composite (V) is only charged in fiber-direction (||), the matrix (M), in this case the honeycomb, and the „fiber“ (F), in this case the aerogel, are loaded parallel (Fig. 6). The model for the calculation of the apparent Young's modulus E|| is therefore based on the addition of the forces at identical deformation Δl. With ε = Δl/l and ($\varphi_{F,M} = A_{F,M}/A_V$), equation II.1 can be derived for the apparent Young's modulus E|| for pure elastic deformation.

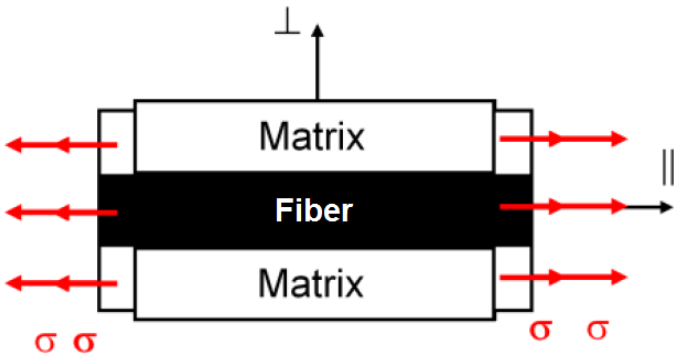


**Fig. 6:** Assumption of parallel linear springs [42]

(Eq. II.1) $$\Leftrightarrow E_{\parallel} = E_{F\parallel} \cdot \varphi_F + E_M \cdot (1 - \varphi_F)$$

Is the composite is loaded perpendicular to the fiber-direction ( $_{\perp}$ ), the same force acts on both the fiber (aerogel) and the matrix (honeycomb) (Fig. 7). This time, the overall deformation is composed of the deformations Δl of the two component materials. Again, after assuming linear elastic behavior, the apparent Young's modulus $E_{\perp}$ can be derived (Eq. II.2). For more details consider [43].

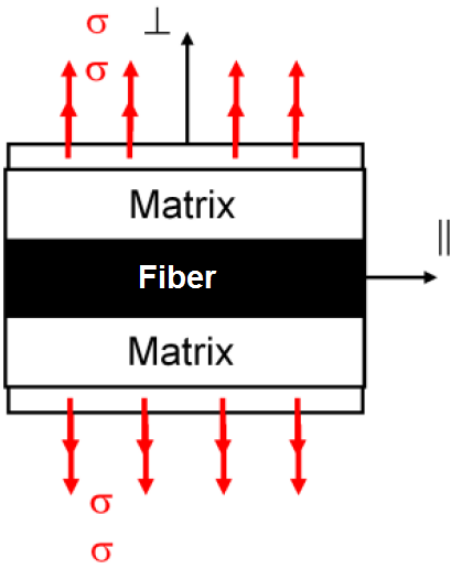


**Fig. 7:** Assumption of perpendicular load [42]

(Eq. II.2) $$\Leftrightarrow E_{\perp} = \frac{E_M \cdot E_{F\perp}}{E_{F\perp} \cdot (1-\varphi_F) + E_M \cdot \varphi_F}$$

Both equations show, that the volume fraction of the honeycomb material and the volume fraction of the aerogel together with their properties in-plane and out-of-plane determine the composite behavior. Both equations give, however, only the upper and lower limit of apparent Young's modulus. In reality all values are in between these two extremes. Other models and bounds have been derived in the literature and more refined models for various arrangements of fibers in a matrix exist [Hull, Summerschool2014]. All rules of mixtures and their improvements rely on assumptions like this [44]:

(1) ideal, parallel alignment of the regular allocated fibers
(2) firm adhesion between fiber and matrix
(3) hardly any defects in the composite
(4) linear elastic behavior of fiber and matrix

The rules of mixtures will be applied to the materials prepared in this thesis.

When assuming the parallel setting, the rule of mixtures can apparently also be easily applied to other properties of composites, such as density or thermal conductivity. Again, the properties of the constituent and their respective volume fraction are needed.

# III. Experimental

In the following section, a description of the research design is given, so that it can be replicated. At first, detailed information on the chemicals and honeycomb is presented. In section B the utilized recipes can be quickly looked up with only a short description for experienced readers. A more detailed description of the synthesis route, covering the aging, drying and characterization process, is discussed in section C.

## A. Used chemicals & honeycomb

For the performed synthesis routes of flexible and inflexible silica-aerogels on TEOS, MTMS and 3-(2,3-Epoxypropoxy)propyltrimethoxysilane GPTMS basis, the chemicals shown in Tab. 2 were used as received.

**Tab. 2:** Tabular listing of the chemicals used

| | Utilized chemicals: | CAS-No.: | Purity: | Manufacturer: |
|---|---|---|---|---|
| **Precursor:** | Tetraethyl orthosilicate (TEOS) | 78-10-4 | > 99% | Merck |
| | Methyltrimethoxysilane (MTMS) | 1185-55-3 | 95% | Sigma-Aldrich |
| | [3-(2,3-Epoxypropoxy)-propyl]-trimethoxysilan (GPTMS) | 2530-83-3 | ≥ 97% | Merck |
| **Surfactant:** | N-(Hexadecyl)trimethyl-ammonium chloride (CTAC) | 112-02-7 | 96% | Alfa Aesar |
| **Solvent:** | Ethanol | 64-17-5 | 96% | Walter CMP |
| | Methanol | 67-56-1 | 98.5% | VWR Intern. |
| **Catalyst:** | Diethylentriamine (DETA) | 111-40-0 | 99% | Alfa Aesar |
| | Ammonia ($NH_4OH$) | 1336-26-1 | 28-30% | Merck |
| | Hydrochloric acid | 7732-18-5 | 10e-4M | Merck |

In order to improve the mechanical properties of the aerogel, the following honeycomb-structures (Fig. 8) with the properties given in (Tab. 3) have been used for strengthening the aerogel. They consist of Nomex paper, expanded and manufactured as discussed in II.b).

**Table 3:** Tabular listing of the aerospace qualified honeycomb used

| Manufacturer: | Utilized honeycomb: | Cell size: | Density: | Compressive strength (stabilised): | Shear modulus (L/W): | Height: | Thermal conductivity: |
|---|---|---|---|---|---|---|---|
| Schütz Industry Services | Core Master C1 | 3.2 mm | 0.029 g/cm³ | 0.75 Mpa | 15 / 11 MPa | 5/10/15mm | 60 mW/mK |
| | Core Master C1 | 6.4 mm | 0.024 g/cm³ | 0.45 Mpa | 13.5 / 9 MPa | 5/10/15mm | 60 mW/mK |
| Hexcel | Hexweb A10 | 5 mm | 0.032 g/cm³ | 1.2 MPa | 29 / 19 MPa | 5/10/20mm | 60 mW/mK |

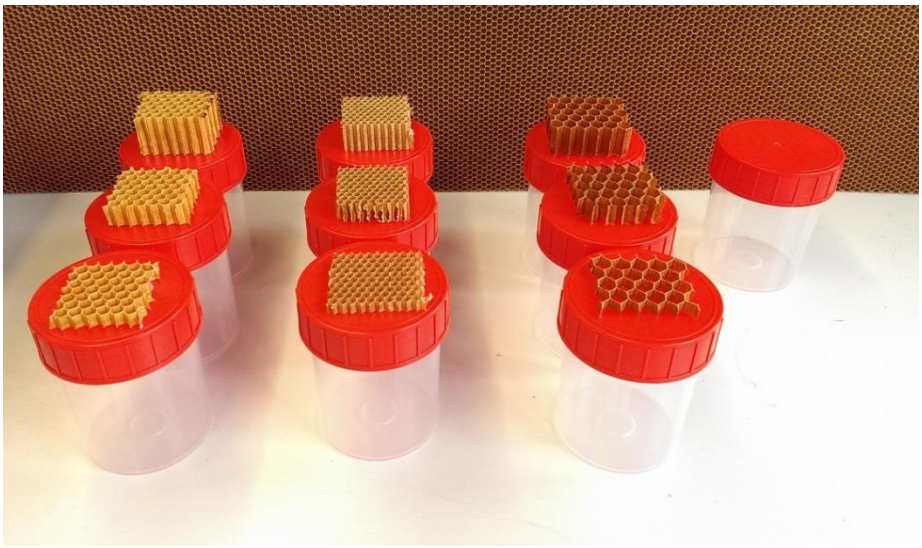

**Fig. 8:** Showcase of the honeycombs used for a test series, showing A10-5, C1-3,2 and C1-6,4 from the left to the right

## B. Applied aerogel recipes

In this subsection the performed synthesis route of each aerogel used is briefly described for experienced readers for look-up. Afterwards the synthesis itself is described in detail in section IV.C.

### i. SA1 (super-flexible MTMS based)

For the synthesis of the super-flexible MTMS-based aerogel named SA1, the chemicals shown in Tab. 4 were used as received. To adjust pH-levels in different steps of the synthesis, 0.0001M HCl and ammonia (28-30%) were used. The molar ratio of MTMS:Methanol:CTAC:$NH_4OH$:HCl was set to 1:35:4:4:4. In a typical synthesis 12.2 g of MTMS was mixed with 100.24g methanol and 2.034g hexadecyl-trimethylammonium chloride CTAC in a beaker. Then 6.445g of a 0.0001M HCl solution was added and stirred for 3 hours being covered with aluminum foil. After that, 12.533g $NH_4OH$ (28-30%) was added to start the condensation. At this time the sample was transferred into an oven at 50°C temperature for aging.

**Tab. 4:** SA1 - required amount of substances

| | Utilized chemicals: | Typical quantity: | Synthesis: |
|---|---|---|---|
| **Precursor:** | Methyltrimethoxysilane (MTMS) | 12.199g | Mix MTMS, Methanol, CTAC and HCl<br>-> cover beaker<br>-> 3 hours stirring |
| **Surfactant:** | N-(Hexadecyl)trimethyl-ammonium chloride (CTAC) | 2.0336g | |
| **Solvent:** | Methanol | 100.24g | ↓ |
| **Catalyst:** | Hydrochloric acid | 6.445g | |
| | Ammonia ($NH_4OH$) (1,5 wt%) | 3.1332g | after 3 hours: add $NH_4OH$<br>-> Aging |

**SA1 - Molar Ratio:** 1:35:4:4:4 (MTMS:Methanol:CTAC:$H_3O^+$:NH4OH)

### ii. SA2 (semi-flexible MTMS & GPTMS based)

For the synthesis of the semi-flexible MTMS & GPTMS-based aerogel named SA2, the chemicals shown in Tab. 5 were used as received. The molar-ratio of MTMS:GPTMS:CTAC:DETA:Methanol:HCl was chosen to be 1:0.25:0.071:0.125:30:30. In a typical synthesis 14.64g of MTMS were mixed with 6.36g of GPTMS in 103.32g methanol and as 2.43g of CTAC added. Then 58.11g HCl was added drop wise in the beaker and the beaker covered with aluminum foil. After 3 hours of stirring, 1.38 g DETA was added and the samples were transferred to an oven at 50°C temperature.

**Tab. 5:** SA2 - required amount of substances

| | Utilized chemicals: | Typical quantity: | Synthesis: |
|---|---|---|---|
| **Precursor:** | Methyltrimethoxysilane (MTMS) | 14.64g | Mix MTMS, GPTMS, Methanol, CTAC and HCl<br>-> cover beaker<br>-> 3 hours stirring |
| | [3-(2,3-Epoxypropoxy)-propyl]-trimethoxysilan (GPTMS) | 6.36g | |
| **Surfactant:** | N-(Hexadecyl)trimethyl-ammonium chloride (CTAC) | 2.43g | |
| **Solvent:** | Methanol | 103.32g | ↓ |
| **Katalyst:** | Hydrochloric acid | 58.11g | after 3 hours: add DETA<br>-> Aging |
| | Diethylentriamin (DETA) | 1.38g | |

**SA2 - Molar Ratio:** 1:0.25:0.071:30:30:0.125 (MTMS:GPTMS:CTAC:Methanol:$H_3O$+:DETA)

### iii. SA3 (inflexible TEOS based)

For the synthesis of the inflexible TEOS-based aerogel named SA3, the chemicals shown in Tab. 6 were used as received. To adjust pH-levels for hydrolysis, hydrochloric acid and diluted ammonium hydroxide (1.5%wt) were used. For the synthesis of this low conductivity aerogel named SA3, the molar ratio of TEOS:Ethanol:HCl was fixed to 1:8:6. In a typical synthesis 34.52 g of TEOS was mixed with 61g solvent and then stirred for 3 hours after adding 17.88g HCl drop wise in the beaker and covered with aluminum foil. Finally after 3 hours, 0.156g ammonium hydroxide solution (1.5%wt) was added and the samples were transferred into an oven at 50°C temperature.

**Tab. 6:** SA3 - required amount of substances

| | Utilized chemicals: | Typical quantity: | Synthesis: |
|---|---|---|---|
| **Precursor:** | Tetraethyl orthosilicate (TEOS) | 34.52g | Mix TEOS, EtOH, HCl<br>-> cover beaker<br>-> 3 hours stirring |
| **Solvent:** | Ethanol | 61g | |
| **Catalyst:** | Hydrochloric acid | 17.88g | |
| | Ammonia ($NH_4OH$) (1,5 wt%) | 0.156g | after 3 hours: add $NH_4OH$<br>-> Aging |

**SA3 - Molar Ratio:** 1:8:6:37 (TEOS:Ethanol:$H_3O$+:$NH_4OH$)

## C. Synthesis - approach & batch preparation

Below the experimental procedure of aerogel synthesis, as carried out for this research, is described in detail. The necessary theoretical background is discussed in chapter II.a.iii). The steps of synthesis (Fig. 9), starting with mixing of precursors followed by the formation of the sol via the alcogel to the final aerogel sample, are similar for each recipe.

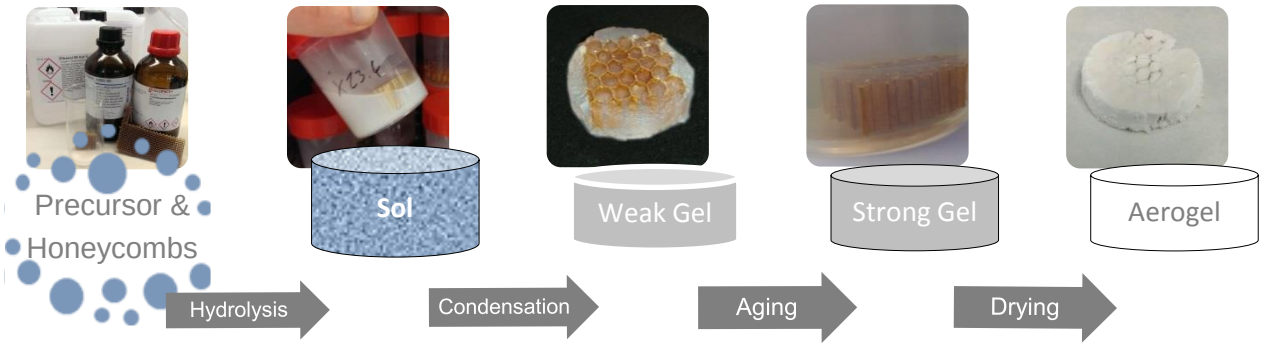


**Fig. 9:** Steps during the aerogel synthesis procedure.

### Honeycomb preparation:

The previously described Nomex-honeycomb products, manufactured by Hexcel and Schütz Industry Services, are used. To ensure comparability, all honeycomb samples were cut in 35mm x 35mm pieces (with variable height of 5,10,15/20mm) with a scalpel. Thus a total of 10 specimens per charge, consisting of three different honeycomb products, each with every available height, plus a single reference sample, were prepared.

### Combination of sol & honeycomb:

The solutions for the aerogels are prepared as described above. Once the solutions are finished with adding the base catalyst, the solution is transferred to the honeycombs and cast into labeled PP beakers (52mm diameter used), which are sealed to allow gelation taking place without evaporation of the volatile components (Tab.7).

**Tab. 7:** Amount of sol per sample filled in the beaker

| Honeycomb typ: | Height: | | |
|---|---|---|---|
| | 5mm | 10mm | 15/20mm |
| C1-3.2 | 30ml | 30ml | 40ml |
| A10-3,2-5 | 25ml | 35ml | 50ml |
| C1-6,4 | 30ml | 30ml | 40ml |

Gelation and aging:

After combining the sols and the honeycombs the filled beakers are placed in the oven for aging, see Tab. 8. Only the samples of SA3 are an exception: For them, the aging time was changed in the course of the experiments. The reasons for this are discussed in section IV.B.i. - Appearance of inflexible SA3-based composites. Aging temperature was set to 50°C for all samples. Linear shrinkage during aging was observed by measuring the diameter of wet gel rods with a caliper before and after aging. All the gels show a low amount of shrinkage (<5%).

**Tab. 8:** Aging time and temperature per aerogel

| Aerogel typ: | Time: | Temperatur: |
|---|---|---|
| SA1 | 5 days | 50°C |
| SA2 | 2 days | 50°C |
| SA3 | 1+2 days / (2 days) | 22°C & 50°C / (50°C) |

Washing:

After gelation and aging, the wet materials are washed with ethanol. Experience has shown that changing the solvent for 5-8 times, once in the morning and once in the late afternoon, yields for good results, namely marginal shrinkage. As a consequence of that, the solvent was changed 8 times for all samples (Tab. 9)

The stiffer alcogels SA2 and SA3 can be carefully retrieved from the beakers and transferred into larger ethanol-filled 400ml PP-beakers. Tests showed better results when using this method, though risking a damaging of the samples when pulling them out, as exemplary shown in Fig. 10 below. SA3 can be easily pressed out of their container. SA2 on the other hand is way more fragile and needs to be separated from the beaker with a needle. Relocating the gels to a large container has the advantage that the gel is enclosed with ethanol from all sides, which accounts for better diffusion out of the gel from all sides.

**Tab. 9:** Washing parameter

| Washing parameter | |
|---|---|
| Solvent: | Ethanol |
| Number of solvent exchanges: | 8 times |
| Solvent exchange schedule: | 2 times a day |
| Storage temperature: | 22°C (lab conditions) |

The SA1 gel however is extremely fragile and has to be handled with great caution. This is the reason why this aged gel cannot be retrieved and has to be washed and later on dried in its beaker. For washing, one has to separate the gel from the beaker with a needle again and carefully exchange the solvent with a pipette.

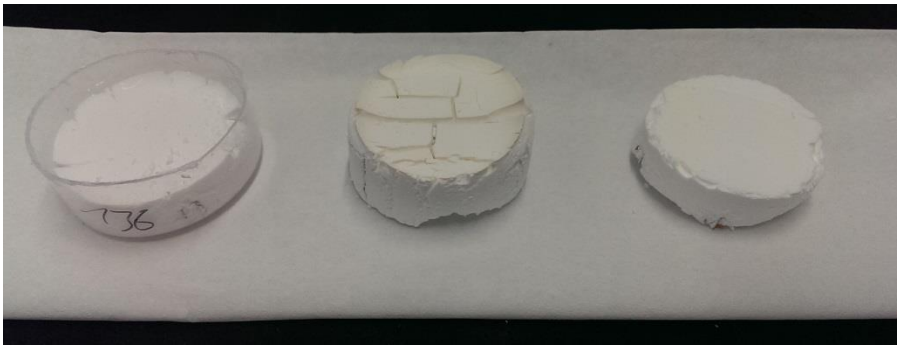

**Fig. 10:** Pictures of three semi-flexible SA2-based composites, the first one being dried in a cut of beaker, the second one in an unprepared beaker and the third one in a paper bag

Supercritical drying:

With the alcogels being washed as described, the next characteristic step for the fabrication of an aerogel is supercritical drying. For better handling it is strongly recommended to pack up the samples SA2 and SA3 into paper or tea bags. This way they can be marked with a pencil and put in the pressure tank of the autoclave along with the in-beaker SA1 specimens.

**Tab. 10:** Parameter for supercritical drying

| Washing parameter | |
|---|---|
| Pressure: | 97 bar |
| Temperature: | 46°C |
| Solvent: | Ethanol (Aceton for SiUF) |
| Duration: | ~50hours |
| Mass flow rate: | ~ 14 kg/hour |

To prevent harmful drying out while starting the autoclave, a determined amount of solvent is added to the samples in the pressure tank in such a way that all specimens are fully submerged. The pressure tank then is closed. After that, the autoclave can be started using the parameters shown in Tab. 10. The cylindrical gel disks were dried in a vertical autoclave ($CO_2$ Extraktionsanlage HPE-LAB-150, Eurotechnica, Germany, 2012) through a direct $CO_2$ supercritical route [27] with a chamber volume of 12 Liters as described in II.a.iv). The replacement of the solvent with $CO_2$ took less than 45h. The first step of drying, consisting in replacing the solvent within the gels with supercritical $CO_2$ by diffusion, was performed dynamically under a constant $CO_2$ flow rate of around ~14 kg/hour. The degree of advancement of the drying was experimentally investigated by withdrawing exchanged solvent from a drainage valve. If no more solvent can be extracted from the separator vessel B2, degassing at a constant rate of 0.1 bar/min was initiated. After reaching ambient pressure, aerogels can be extracted.

A summary of the synthesis is given in figure 11.

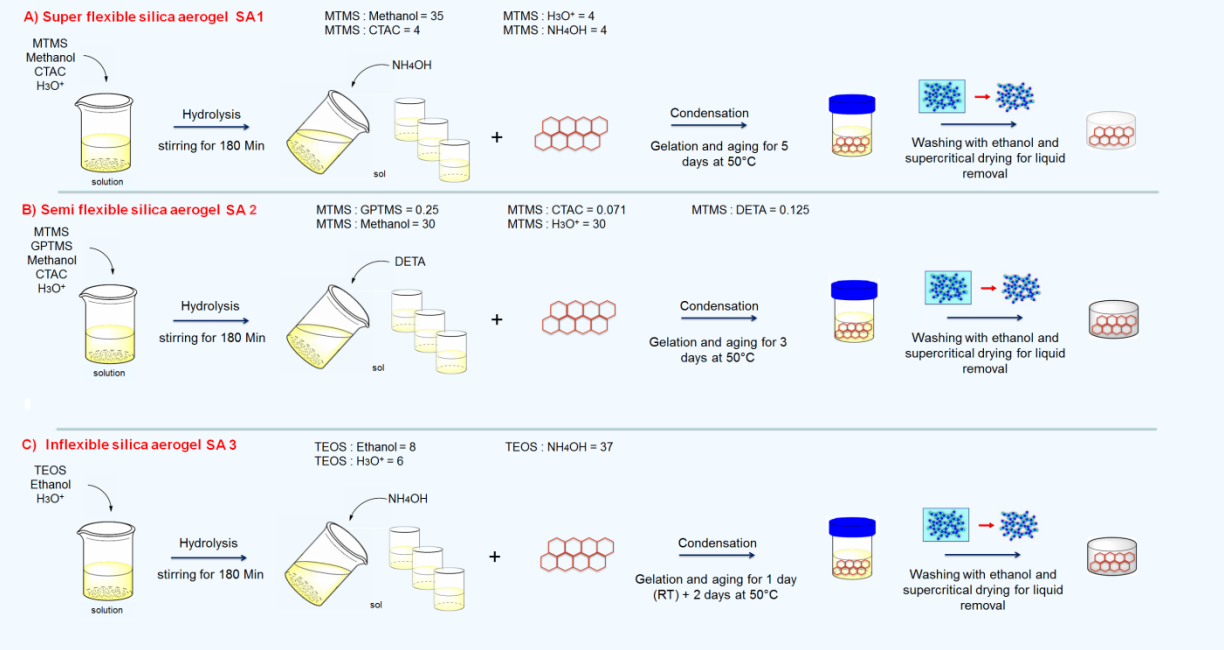


**Fig. 11:** Outline of the different synthesis-routes, from precursors to final samples

## D. Characterization Methods

### i. Motivation for the chosen characterization methods

The aim of the current explorative research was to find ways to improve the mechanical stability of silica aerogels utilizing aramid-honeycombs as a stabilizing backbone. Focusing on thermal insulation, not only brittleness had to be reduced. Thermal conductivity still should be in a competitive range to other materials.

Therefore the analysis was focused on these two aspects, thermal conductivity and mechanical stability, enriched with complementing data on density, mass and volume fraction and specific surface area and shrinkage. In this context, the Transient Plane Source (TPS) method was used being one measurement method for thermal conductivity. For the characterization of the mechanical properties, a standard in-plane and out-of-plane compression test provided the desired information on the apparent Young's modulus, which is a most simple but still characteristic value to obtain. Covering the specific surface area, insightful subsidiary information is provided, too. Another important quality of both aerogels and materials in a composite is shrinkage, which was measured and noted as well. At last, more general properties like appearance and adhesion between the components and the density were investigated.

### ii. Sample preparation

The specimens were pulled out of the beakers or paper bags in which they have been supercritically dried. For better measurements, the specimens are then cut into a cuboid form by abscising the pure aerogel layers around the aerogel-honeycomb-composite-block. Henceforth the samples can be studied. The dimensions of each specimen are measured and its weight is recorded. Photos of this sample shape are taken, due to the destructive kind of the measurement of mechanical properties.

### iii. Measurement of density, volume percentage and shrinkage

The density of the composites and pure aerogels was measured with two different methods: Not only from their volume and mass, but also via Micromeretics' Geopyknometer 1360 comparative data were obtained.

The first technique makes use of the well measurable geometry, especially of the rectangular aerogel-honeycomb-compound. Given its volume (via quantifying its length, width and height with the assumption of ± 1mm absolute error using a digital caliper), density can easily be

calculated by dividing by the composite's weight (assuming ± 0,01 g absolute error using a laboratory balance). The same procedure can be used to check the pure aerogel reference sample density. This method is inaccurate, with margin of error of approximately 8-18%.

For the second technique first a small amount of custom-made finely ground quartz glass sand is compressed with a given force in a cylinder. The volume of the sand is then determined by using the covered distance of the compressing piston compared to the force. Now the actual sample is weighted and added. The finely granulated siliceous sand is optimized to totally enclose the sample like a liquid, so that the new combined volume is determined in the next compression cycle (same force applied) via the difference of covered distance. Then, with the weight already being attained, the difference of the measured volumes, thus the sample volume, allows the calculation of the density (reproducibility ± 1.1% when sample volume is at least 25% of sample holder) of the aerogel.

Furthermore, given a previously noted weight of the honeycomb in each sample, the weight percentage of aerogel in each composite can be easily determined by subtracting the honeycomb weight from the total weight. Hereinafter the volume percentage of the aerogel can be calculated combining the obtained information about weight percentage and the density of the aerogel.

Additionally, volume shrinkage was determined via equation (III.1) with the approximate sample volume before and after supercritical drying with V1 and V2 being the volumes of alcogel and aerogel respectively. Therefore, the diameter and height of the monolithic aerogel blocks were measured in the beakers before and after aging as well as supercritical drying, so that the intrinsic shrinkage of the aerogel itself can be recorded.

(Eq. III.1) $$Shrinkage\ (\%) = \left(1 - \frac{V2}{V1}\right)\ x\ 100$$

### iv. Thermal conductivity measurement via Hot Disk

There are many different types of instruments for thermal conductivity measurements available, based on different principles. This section will give a brief theoretical description of the Hot Disk Thermal Constants Analyzer TPS2500, which is not an ASTM-standardized (American Society for Testing Materials) testing method. For more details see [45].

Based on the theory of the Transient Plane Source technique [46], this device utilizes a sensor element in the shape of a double spiral which allows testing of both anisotropic and isotropic

materials (Fig. 12). Whilst being placed between two samples, a constant electrical current flow is conducted through the spiral, which causes a transient temperature increase of the sensor and the near sample surroundings. At a rate depending on the thermal transport properties of the material, the generated heat dissipates into the sample. Therefore the sensor-element acts both as a heat source for increasing the temperature of the sample as well as an electrical resistance linked transducer for recording the time dependent temperature increase. These recordings allow the calculation of the thermal transport properties of the sample. It is precisely designed with exact width, number of windings and windings radii, which accounts for the needed accuracy for calculations. Its 10µm thick spiral is made of Nickel, covered by the polyimide Kapton to protect its shape, give it mechanical strength and keep it electrically insulated in the temperature range from 10K to 500K [47].

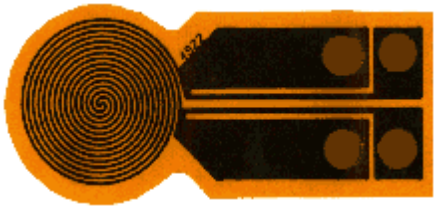

**Figure 12:** Nickel-double-spiral sensor covered in Kapton [48]

For testing, the encapsulated Ni-spiral sensor (Fig. 12) is sandwiched between two halves of solid, coplanar, chemically and geometrically identical, weighted and sized samples. The samples were previously degased over night to withdraw any moisture, which worsens the measurement, and to set shared initial conditions, independent from the ambient conditions. A weight is then placed on top of the buildup to ensure a sufficient contact between the sensor and the sample surface. Finally the setup is covered by a metal cap to avoid disturbances by air flows (Fig. 13). Then parameters, like the applied power increasing the temperature of the spiral, the “Measuring Time”, the size of the sensor or the room temperature, are adjusted to optimize the settings for the experiment so that thermal conductivities from 0.005-500 W/mK can be measured. S.E Gustafsson et al. have shown that the accuracy of measurements over a wide range of thermal conductivities is within ± 5% and the reproducibility is within ± 2% [49].

**Figure 13:** Test set-up of the Hot-Disk-installation with metal cap [48]

While evaluating the statistical data it is important to keep an eye on the distance between the sensor and the end of the probe. The probing depth, caused by the heating parameters time and power, has to be smaller than the probe dimensions, otherwise the results are defective. Furthermore the minimum testing time has to excel a specific value to ensure a significant measurement. Being below the approved values is highlighted by color. When a set of data is attained, the resulting plot still has to be fitted to discard irrelevant outliers. In consequence of that, tables of the thermal conductivity results, the specific heat and thermal diffusivity are obtained.

### v. Measurement of mechanical properties - Compression test

The compression tests were carried out with a compression machine (Latzke, Germany) which determines mechanical properties under homogeneous uniaxial loads by recording force-deformation curves. For more detailed information consider the text book Mechanical Metallurgy by Dieter [50].

The line of action is as follows: To guaranty that the front surfaces of the sample are parallel and perpendicular to the sample axis, some of them have been polished with abrasive paper (Grit 500/P1000) if needed. The previously sized specimens are placed between two parallel plates. Then the parameters like size and max force are preset. When starting the operation, the compression raises slowly at constant compression velocity of 1mm/min charging the

sample with an uniaxial load. At the same time, the corresponding force F is measured. As a general rule, the quadratic specimens were compressed to 50% of the original length in-plane and out-of-plane. In Figure 14, the compression test is schematically shown. The data then are converted to compression stress σ and relative compression strain ϵ, from which the apparent Young's modulus results from the initial slope of the stress–compression curve.

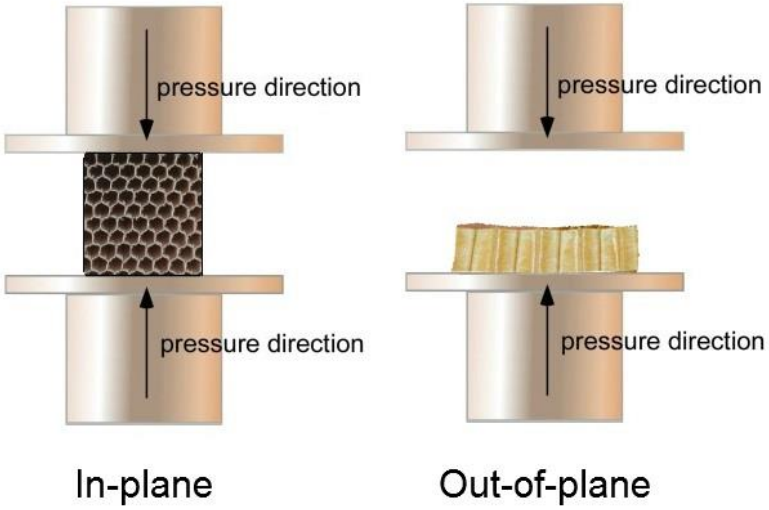


**Fig. 14.:** Schematic drawing of the In-plane and Out-of-plane compression test.

vi. SEM - Scanning electron microscopy

To get information on the nanostructure of the aerogels' and composites', especially the binding between the aramid honeycomb and the aerogel, SEM images were recorded with a scanning electron microscope type Merlin by Carl Zeiss SMT, using the detector for secondary electrons (Fig. 15). SEM pictures of electrically insulating materials from their fractured surfaces require a coating with a thin layer of gold prior to observation in order to reduce the effect of charging [51]. The coated samples are transferred to the sample chamber. For further details on SEM, consult authors like Goldstein et. al. [52].

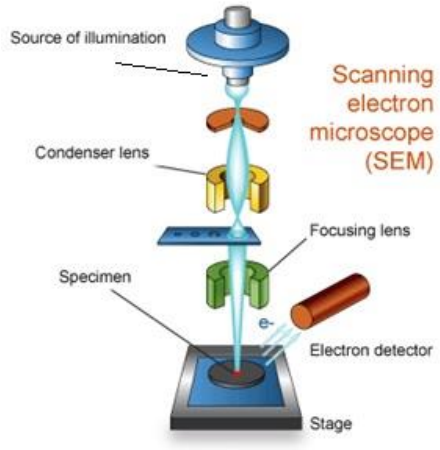


**Fig. 15:** Schematic drawing of a SEM. [16]

### vii. BET - Measurement of the specific surface area

The BET-method is an analytical technique to determine the specific surface area of porous materials by nitrogen sorption analysis. BET stands for the artificers S.Brunauer, R.H. Emmett and E. Teller. The specific surface area of the aerogels used was determined by $N_2$ adsorption at the boiling point of liquid nitrogen (77.3K) via the BET equation [54] using a Tristar II 3020 built by Micromeritics, Norcross, USA. Pores with a diameter above 100 nm are not considered in this calculation. A more detailed discussion of the method is done by Himmel et. al. [55].

At first, purpose-built glass tubes, which will contain the samples later on, are weighted empty. Before measuring the samples it is necessary to degas them. For this reason, the small samples of around 0.1 g are placed in the tubes and are put under vacuum over night at 110 °C. This reduces the amount of moisture and other possibly adsorbed species. On the following day, the net weight of the samples can be obtained by weighing their tubes again and subtracting the obtained tube-weight. Afterwards, the sample containing tubes can be placed in the analyzer and are automatically submerged into a bath with liquid nitrogen (−196 °C). Then the measurement begins. It is based on the fact that nitrogen gas, which is injected in the tubes stepwise, gas bound at the pore walls by van der Waals interaction. Because of this adsorption, the relative gas pressure in the sample drops in comparison to the empty tube. For this reason the relative gas pressure $p/p_0$, with p = nitrogen partial pressure and $p_0$ = saturation pressure, can be plotted against the specific amount adsorbed, given in $cm^3/g$. In

summary, this gives the essential Isotherm-plot for adsorption and desorption stepwise, which then contains information about the sample measured.

Besides the specific surface area, BET can give access pore radii distribution. The related BJH-method on the other hand was originally designed for relatively wide-pore adsorbents with a wide pore size distribution [56].

# IV. Results and discussion

Each recipe, flexible SA1, semi-flexible SA2 and inflexible SA3, could be combined with the honeycomb used. For the first two composites, based on flexible SA1 and semi-flexible SA2, suitable adherence and thermal conductivities of 0.036-0.041 W/mK and 0.0395-0.0455 W/mK could be measured. Honeycomb dependent apparent Young's moduli of up to 0.137 MPa in-plane / 21.13 MPA out-of-plane for SA1 such as 0.16 MPa in-plane / 20.16 MPA out-of-off plane for SA2 could be found. The results confirm the expectation, that the aramid honeycomb have a low effect (~10-15% increase) on the thermal conductivities of the aerogel composites. The mechanical properties are increased clearly (represented by the apparent Young's modulus, which increased in the magnitude of >1000 for SA1 and in the magnitude of >100 for SA2 out-of-plane compression).

This section covers all the final results and their discussion. At first data sheets on each recipe are given, which summarize the essentials of the data obtained. Secondly the key features of the composite are analyzed, followed by a section exposing complementary data. Finally, the discussion of the results covers conclusions, challenges, approaches to these challenges and possible opportunities.

## A. Data

In this subsection, the obtained raw data of the most favorable specimen are exhibited in table form (Tab. 11-17). All the other non-listed samples suffered from failures during fabrication, for example due to improper drying at Separex, France, or failures from bubbles and shrinkage.

**Tab. 11**: Datasheet 1 of the SA1-based samples (35x35mm preform)

| Sample: | | .-0152 | .-0153 | .-0154 | .-0155 | .-0156 | .-0157 | .-0158 | .-0159 | .-0160 | .-0161 |
|---|---|---|---|---|---|---|---|---|---|---|---|
| Cell-Configuration: | | Reference | C1-3,2 5mm | C1-3,2 10mm | C1-3,2 15mm | A10-5,2 5mm | A10-5,2 10mm | A10-5,2 20mm | C1-6,4 5mm | C1-6,4 10mm | C1-6,4 15mm |
| Degree of deformation (%): | | <5% | 11,6 | 13,5 | 9,5 | 7,7 | 13,8 | 8,1 | 12,5 | 5,2 | 12,1 |
| Density (kg/m³): | | ~37 / -* | 74 | 64 | 71 | 71 | 71 | 72 | 66 | 55 | 66 |
| Aerogel mass fraction (+/-2%): | | 100 | 64,41 | 62,91 | 59,38 | 68,73 | 55,1 | 53,3 | 76,01 | 58,2 | 59,1 |
| Aerogel volume fraction** (%): | | 100 | 92,7 | 92,7 | 92,7 | 95 | 95 | 95 | 96,2 | 96,2 | 96,2 |
| Thermal Conductivity (+/-1 mW/mK): | | 34 | 38 | 38,5 | 40 | 41 | 39 | 39 | 38 | 36 | 39 |
| in-plane: | Young's modulus (MPa) | 0,0025 | - | - | - | - | - | - | - | - | - |
| out-of-plane: | | 0,0025 | 7,63 | 10,2 | 11,38 | 10,73 | 13,58 | 21,13 | 6,45 | 10,48 | 12,67 |
| BET (+/-1 m²/g): | | 435,6 | 435,6 | 435,6 | 435,6 | 435,6 | 435,6 | 435,6 | 435,6 | 435,6 | 435,6 |
| Note: | | | | | | | | | | | |

* : Geopyc. Density ** theoretically

**Tab. 12**: Datasheet 2 of the SA1-based samples (35x35mm preform)

| Sample: | .-0162 | .-0163 | .-0164 | .-0165 | .-0166 | .-0167 | .-0168 | .-0169 | .-0170 | .-0171 |
|---|---|---|---|---|---|---|---|---|---|---|
| Cell-Configuration: | Reference | C1-3,2 5mm | C1-3,2 10mm | C1-3,2 15mm | A10-5,2 5mm | A10-5,2 10mm | A10-5,2 20mm | C1-6,4 5mm | C1-6,4 10mm | C1-6,4 15mm |
| Degree of deformation (%): | <5% | 8,1 | 14,2 | 10,6 | 9,3 | 13,2 | 17 | 7 | 13,5 | 8,4 |
| Density (kg/m³): | ~37 / -* | 64 | 74 | 67 | 77 | 70 | 75 | 65 | 62 | 57 |
| Aerogel mass fraction (+/-2%): | 100 | 75,25 | 62,59 | 58,82 | 64,39 | 58,94 | 53,02 | 72,51 | 61,37 | 52,63 |
| Aerogel volume fraction** (%): | 100 | 92,7 | 92,7 | 92,7 | 95 | 95 | 95 | 96,2 | 96,2 | 96,2 |
| Thermal Conductivity (+/-1 mW/mK): | 34 | 38 | 38,5 | 40 | 41 | 39 | 39 | 38 | 36 | 39 |
| in-plane: Young's modulus (MPa) | 0,0025 | - | 0,066 | 0,054 | 0,098 | 0,107 | 0,137 | 0,031 | 0,028 | 0,038 |
| out-of-plane: Young's modulus (MPa) | 0,0025 | - | - | - | - | - | - | - | - | - |
| BET (+/-1 m²/g): | 435,6 | 435,6 | 435,6 | 435,6 | 435,6 | 435,6 | 435,6 | 435,6 | 435,6 | 435,6 |
| Note: | | | | | | | | | | |

* : Geopyc. Density ** theoretically

**Tab. 13**: Datasheet 1 of the SA2-based samples (35x35mm preform)

| Sample: | .-0132 | .-0133 | .-0134 | .-0135 | .-0136 | .-0137 | .-0138 | .-0139 | .-0140 | .-0141 |
|---|---|---|---|---|---|---|---|---|---|---|
| Cell-Configuration: | Reference | C1-3,2 5mm | C1-3,2 10mm | C1-3,2 15mm | A10-5,2 5mm | A10-5,2 10mm | A10-5,2 20mm | C1-6,4 5mm | C1-6,4 10mm | C1-6,4 15mm |
| Degree of deformation (%): | ~15%*** | - | 19,4 | 16,4 | 5,2 | 7,8 | 6,7 | 2,7 | 10,2 | 6,2 |
| Density (kg/m³): | - / 91.8* | - | 84 | 87 | 82 | 91 | 99 | 92 | 94 | 96 |
| Aerogel mass fraction (+/-2%): | 100 | - | 72 | 71 | 68 | 68 | 68 | 77 | 76 | 75 |
| Aerogel volume fraction** (%): | 100 | 92,7 | 92,7 | 92,7 | 95 | 95 | 95 | 96,2 | 96,2 | 96,2 |
| Thermal Conductivity (+/-1 mW/mK): | 38*** | 43 | 44 | 45,5 | 52 | 44 | 46 | 41 | 39,5 | 44 |
| in-plane: Young's modulus (MPa) | 0.074 | - | - | - | - | - | - | - | - | - |
| out-of-plane: Young's modulus (MPa) | 0.074 | - | 12,11 | 14,31 | 8,93 | 13,34 | 20,16 | 6,71 | 8,46 | 13,66 |
| BET (+/-1 m²/g): | 359,4 | 359,4 | 359,4 | 359,4 | 359,4 | 359,4 | 359,4 | 359,4 | 359,4 | 359,4 |
| Note: | *damaged* | *Exhibition-sample* | | | | | | | | |

* : Geopyc. Density ** theoretically ***Literature

**Tab. 14**: Datasheet 2 of the SA2-based samples (35x35mm preform)

| Sample: | .-0142 | .-0143 | .-0134 | .-0145 | .-0146 | .-0147 | .-0148 | .-0149 | .-0150 | .-0151 |
|---|---|---|---|---|---|---|---|---|---|---|
| Cell-Configuration: | Reference | C1-3,2 5mm | C1-3,2 10mm | C1-3,2 15mm | A10-5,2 5mm | A10-5,2 10mm | A10-5,2 20mm | C1-6,4 5mm | C1-6,4 10mm | C1-6,4 15mm |
| Degree of deformation (%): | ~15%*** | 17,2 | 26,1 | 13,3 | 9,3 | 9,9 | 11,1 | 9,4 | 5,6 | 3,2 |
| Density (kg/m³): | - / 91.8* | 90 | 103 | 93 | 84 | 95 | 92 | 88 | 86 | 91 |
| Aerogel mass fraction (+/-2%): | 100 | 75,43 | 72,87 | 71,3 | 69,37 | 66,04 | Mrz 00 | 80,15 | 74,84 | 73,68 |
| Aerogel volume fraction** (%): | 100 | 92,7 | 92,7 | 92,7 | 95 | 95 | 95 | 96,2 | 96,2 | 96,2 |
| Thermal Conductivity (+/-1 mW/mK): | 38*** | 43 | 44 | 45,5 | 52 | 44 | 46 | 41 | 39,5 | 44 |
| in-plane: Young's modulus (MPa) | 0,074 | 0,083 | 0,120 | 0,110 | 0,120 | 0,140 | 0,160 | 0,059 | 0,067 | 0,074 |
| out-of-plane: | 0.074 | - | - | - | - | - | - | - | - | - |
| BET (+/-1 m²/g): | 359,4 | 359,4 | 359,4 | 359,4 | 359,4 | 359,4 | 359,4 | 359,4 | 359,4 | 359,4 |
| Note: | | | | | | | | | | |

* : Geopyc. Density ** theoretically ***Literature

**Tab. 15**: Datasheet 1 of the SA3-based samples of the “50+”-series(35x35mm preform)

| Sample: | .-0051 | .-0052 | .-0053 | .-0054 | .-0055 | .-0056 | .-0057 | .-0058 |
|---|---|---|---|---|---|---|---|---|
| Cell-Configuration: | A10-5,2 5mm | C1-3,2 10mm | C1-6,4 15mm | Reference | A10-5,2 5mm | C1-3,2 10mm | C1-6,4 15mm | Reference |
| Degree of deformation (%): | <5% | - | - | - | - | - | - | - |
| Density (kg/m³): | 0,11 / 0,1076* | - | - | 0,1 | 0,11 | 0,11 | - | 0,1 |
| Aerogel mass fraction (+/-2%): | 69 | - | - | 100 | 70 | 76 | - | 100 |
| Aerogel volume fraction** (%): | 95 | 92,7 | 96,2 | 100 | 95 | 92,7 | 96,2 | 100 |
| Thermal Conductivity (+/-1 mW/mK): | - | - | - | 24,4 | - | ~48.6 | - | 24,4 |
| BET (+/-1 m²/g): | 892,1 | 892,1 | 892,1 | 892,1 | 892,1 | 892,1 | 892,1 | 892,1 |
| Note: | | *exhibiton sample* | *damaged* | | | | *exhibiton sample* | |

**Tab. 16**: Datasheet 1 of the SA3-based samples of the “sf”-series(35x35mm preform)

| Sample: | .-0118 | .-0119 | .-0120 | .-0121 | .-0122 | .-0123 | .-0124 |
|---|---|---|---|---|---|---|---|
| Cell-Configuration: | Reference | C1-3,2 10mm | C1-3,2 15mm | A10-5,2 5mm | A10-5,2 20mm | C1-6,4 5mm | C1-6,4 10mm |
| Degree of deformation (%): | <5% | 5,2 | 3,9 | 0,1 | 3,3 | 0,7 | 0,3 |
| Density (kg/m³): | 120 / 133,5* | 93 | 75 | 150 | 102 | 142 | - |
| Aerogel mass fraction (+/-2%): | 100 | 72 | 62 | 77 | 66 | 82 | - |
| Aerogel volume fraction** (%): | 100 | 92,7 | 92,7 | 95 | 95 | 96,2 | 96,2 |
| Thermal Conductivity (+/-1 mW/mK): | 27,9 | - | - | - | - | - | - |
| BET (+/-1 m²/g): | 1028,66 | 1028,66 | 1028,66 | 1028,66 | 1028,66 | 1028,66 | 1028,66 |
| Note: | | *bad adhesion* | *damaged* | *damaged* | *damaged* | *damaged* | *damaged* |

* : Geopyc. Density ** theoretically

**Tab. 17**: Datasheet 2 of the SA3-based samples of the “sf”-series(35x35mm preform)

| Sample: | .-0125 | .-0126 | .-0127 | .-0128 | .-0129 | .-0130 | .-0131 |
|---|---|---|---|---|---|---|---|
| Cell-Configuration: | Reference | C1-3,2 10mm | C1-3,2 15mm | A10-5,2 5mm | A10-5,2 20mm | C1-6,4 5mm | C1-6,4 10mm |
| Degree of deformation (%): | <5%* | 8 | 5,8 | 6,4 | - | - | - |
| Density (kg/m³): | 120 / 133,5* | 99 | 97 | 155 | - | - | - |
| Aerogel mass fraction (+/-2%): | 100 | 72.03 | 70.65 | 77.77 | - | - | - |
| Aerogel volume fraction** (%): | 100 | 92,7 | 92,7 | 95 | 95 | 96,2 | 96,2 |
| Thermal Conductivity (+/-1 mW/mK): | 27,9 | ~48.6 | - | - | - | - | - |
| BET (+/-1 m²/g): | 1028.66 | 1028,66 | 1028,66 | 1028,66 | 1028,66 | 1028,66 | 1028,66 |
| Note: | | *bad adhesion* | *damaged* | *damaged* | *damaged* | *damaged* | *damaged* |

* : Geopyc. Density ** theoretically

## B. Discussion of the features of the composite

### i. Appearance, densities, volume percentage and shrinkage

#### Appearance - super flexible SA1-based composites

The resulting composite, consisting of super-flexible SA1 and reinforcing aramid honeycomb, is displayed in Fig. 15. The pure SA1 aerogel is plain white and extremely fluffy. When slightly blowing over its surface, aerogel powder comes off and one can hardly feel any counterforce when compressing it by hand. Shrinkage was not noteworthy high, estimated to be <5%[2], and therefore neglected in further considerations. In the composite, the SA1 shows sound adhesion on the honeycomb and surrounds it thoroughly without any cracks or major pores. This is important, considering the encountered problems with air bubbles and cracks which deteriorate the inflexible SA3 samples. One can assume that slower gelation, rather in the time span of hours than a few ten minutes, and a more flexible network contribute to a more monolithic structure by allowing gases from the honeycomb to leave when heated.

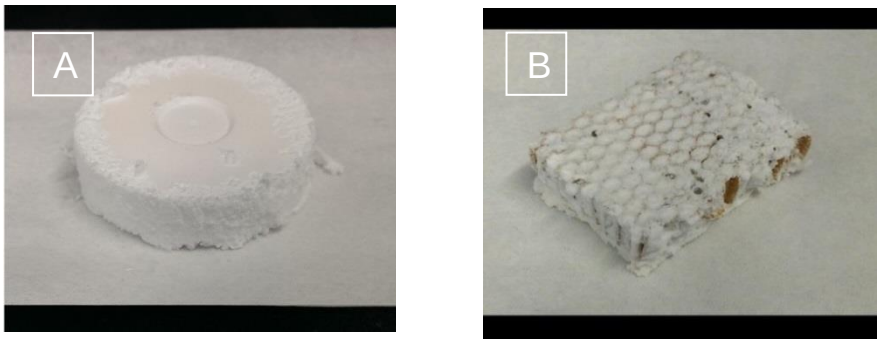


**Fig. 15:** Pictures of a pure SA1-reference-sample (A) and a C1-3,2-10mm-based composite (B)

#### Appearance - semi flexible SA2-based composites

The semi-flexible SA2 aerogel (Fig.16) is a way stiffer than the SA1. Being white as well, with a haptic similar to rubber, it is still somewhat flexible and compressible. Though being significantly more solid than SA1, it is still easy to break off pieces. Previous testing showed a shrinkage of approximately 15% for SA2 [57], which probably causes a deformation of the honeycomb in the composite, as described below. However, no other negative effects can be discovered and adherence is still good. A characteristic feature of the aerogel is its ability to

[2] regarding shrinkage equation Eq.III.1 section III.C.iii)

recover a strain of up to 70% without being damaged, shown in Figure 17 [58]. When it comes to the composite, the aerogel exhibits an even better adherence and encloses it thoroughly without any cracks or large pores. But also the reduced flexibility becomes noticeable in the composite: When taking a close look, small crazes and pores of a few microns can be found, hardly detectable by eye. They both will show negative effects on mechanical and thermal properties.

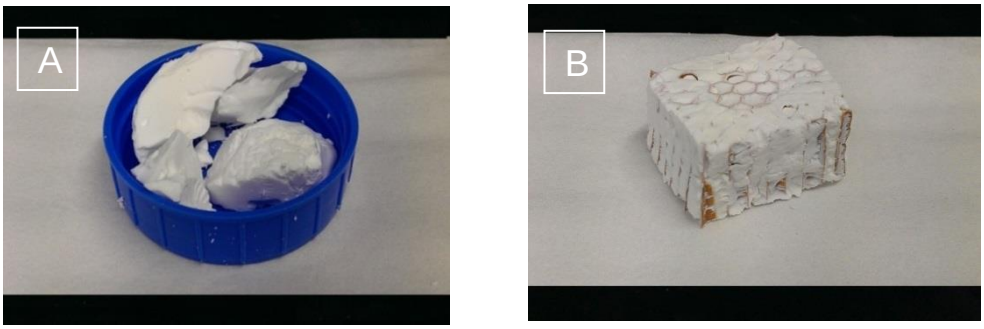


**Fig. 16:** Pictures of a pure SA2-reference-sample (A) and a C1-3,2-10mm-based composite (B)

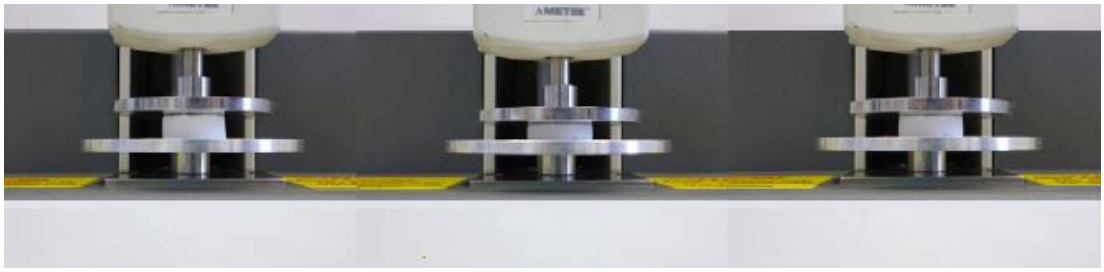

**Fig. 17:** Photograph of the aerogel demonstrating flexibility [No.8]

### Appearance - inflexible SA3-based composites

In contrast to the other recipes, the inflexible SA3-aerogel is not white, but translucent and glassy. It is comparably stiff, though exceptionally brittle, which results in a totally different haptic impression of the surface. When shearing this pure aerogel, it breaks easily, crumbling into smaller pieces with a somehow glassy sound. Shrinkage was measured as described in III.D.ii) with a caliper. First results suffered from high shrinkage and air bubbles, which arose from the surface of the honeycomb, caused by different surface tensions of solid and solvent

(Fig. 18). Pieces of aerogel, from the edge or from the inner cells of the honeycomb, simply drop out when handling the item. Deformation and shrinkage, resulting from the manufacturing process, appear in the form of large cracks and gaps between the aerogel and the honeycomb, when the contracting aerogel separates from the wall. As a result, substantial shrinkage of over 20% necessitated changes in the synthesis. Therefore the routine was changed to a slower aging process (named „sf“), as described in section III.c). The negative effects could be diminished, but not extinguished. The best results (Fig. 19) showed no bubbles and only small cracks and were the result of a vastly increased washing time. But after all, the aerogel still adheres badly to the honeycomb. Before the drying process, the internal space of the honeycomb structure was filled with wet-gel in all samples. Therefore it can be assumed that the shrinkage of the aerogel during supercritical drying is responsible for the problems. Minimizing the shrinkage is very important in controlling the fabrication of aerogel composites. Anyhow, the bad characteristics suggest a discussion about the chance of success when utilizing SA3, which is done in subsection IV.C). In any case, the results obtained are not qualified for further thermal and mechanical testing.

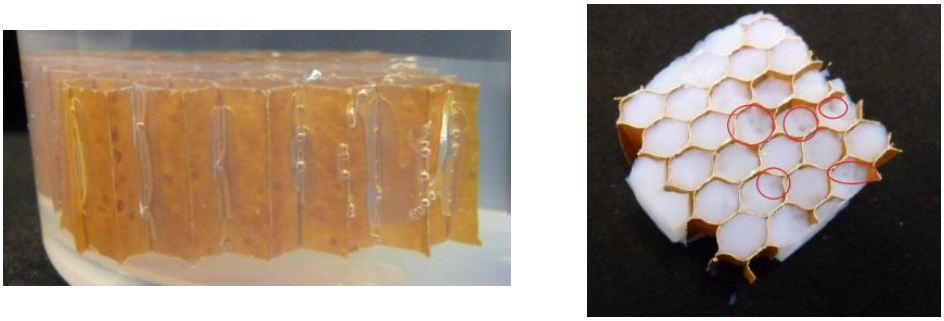

**Fig.18:** Early SA3-based samples, suffering from arising gas bubbles escaping from the honeycomb when heated in the course of aging

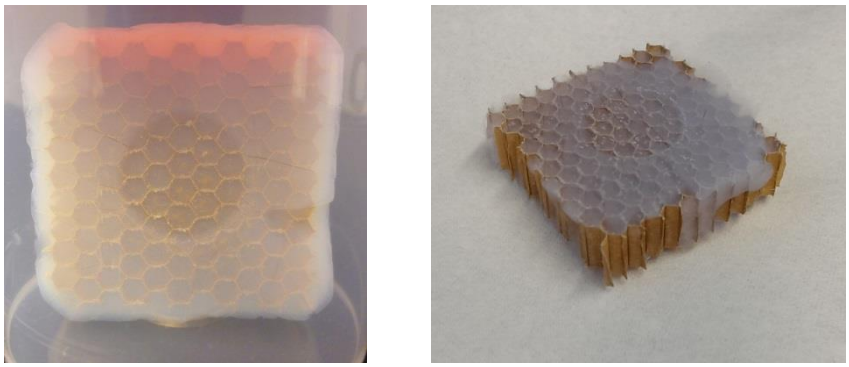

**Fig.19:** Best SA3-based samples synthesized, showing no visible bubbles and close to no cracks

### Appearance - Shrinkage and bending of honeycomb

The most striking effects regarding the appearance of the composite are a strange bending or a distortion of the structure-giving honeycomb. This occurred not before, but after the supercritical drying and scales with the flexibility of the aerogels used.

To quantify and visualize these effects in the data, a so-called „degree of deformation (%)“ is introduced in the data sheets in section IV.A). This should help the reader to get a feeling for the deformation. It is calculated in the following way:

$$\%=\frac{1}{2}*\left[100-\left(\frac{W_{\text{after drying}}}{W_{\text{original}}}\right)*100\right]+\left[100-\left(\frac{L_{\text{original}}}{L_{\text{after drying}}}\right)*100\right] \quad \text{(Eq. IV.1)}$$

$$\text{with } W_{\text{original}} = L_{\text{original}} = 35\text{mm being width and length of the sample before drying}$$

Given Eq.IV.1, the degree is the arithmetic average of the deformations in both length and width of the sample after the synthesis in comparison to the original honeycomb size. However, this does not quantify the described bending.

An example for the described distortion is the inflexible-SA3-based composite, shown in Fig. 20 (A) below. This effect probably increases inner tensions leading to cracks. Given that the honeycombs can normally bear substantial stresses without deforming, noteworthy forces must affect the composite in the autoclave to deform the sample. The assumption is made that especially the inflexible aerogels suffer from the occurring „movement“ and the interaction with the honeycomb during the supercritical drying process. This could explain resulting cracks in the SA3-based composite, though pure aerogel reference samples from the same batch show

no cracks or bubbles. Additionally, the accrued tensions from the elastic forming of the honeycomb are “frozen” by the aerogel, when it is getting stiffer throughout the drying, which causes additional undesirable inner tensions in the final material.

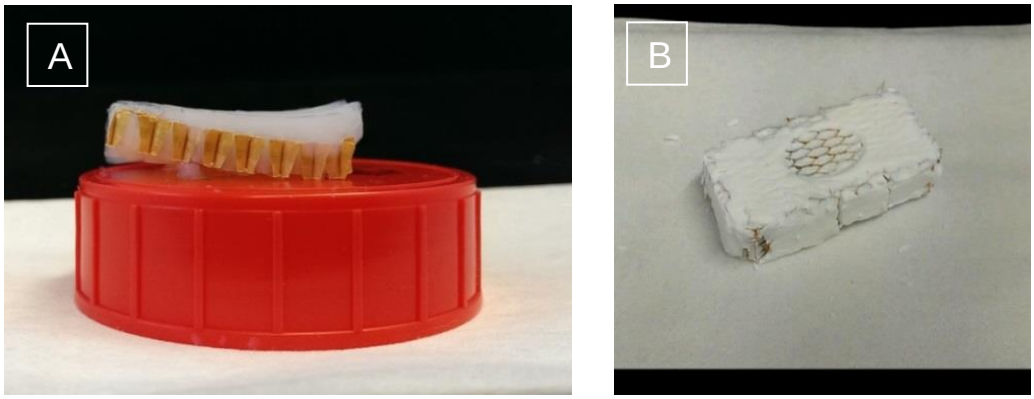


**Fig. 20:** Pictures of a SA3-based bending C1-3,2-5mm composite on the left (A) and the most contracted honeycomb found, enclosed with semi-flexible SA2 aerogel (B)

In comparison, the more flexible the aerogel is, the more it seems to tolerate the arising tensions. Some of the originally 35x35mm sized honeycomb, used for the semi-flexible SA2-based composites, show a contraction in the H-direction (Fig. 20 (B)), as defined in chapter II.B). Apparently, the reason for this distortion of the honeycomb reinforced composites is the relatively high amount of shrinkage (~15%) of the aerogel. At the same time, this distortion was not representative: Other samples of the batch showed smaller or no distortion at all (Fig. 21). No correlation to the sort of honeycomb could be found. Reasons for this effect are discussed in section IV.C).

The composites based on the super-flexible SA1 on the other hand showed no such bending.

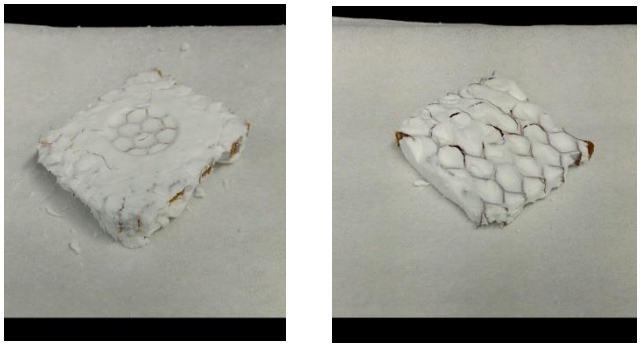

**Fig. 21:** Pictures of two semi-flexible SA2-based composites, which show nearly no contraction, though being produced in the same batch as distorted samples

### Density

Density was determined in two different ways as described in III.D.ii). At first, the density of the "stiff" aerogels' was determined using a Geopyknometer. Additionally the composites density can be measured via its geometry and weight. Using this data, the following graph can be generated (Fig. 22), in which density is plotted against height for all samples.

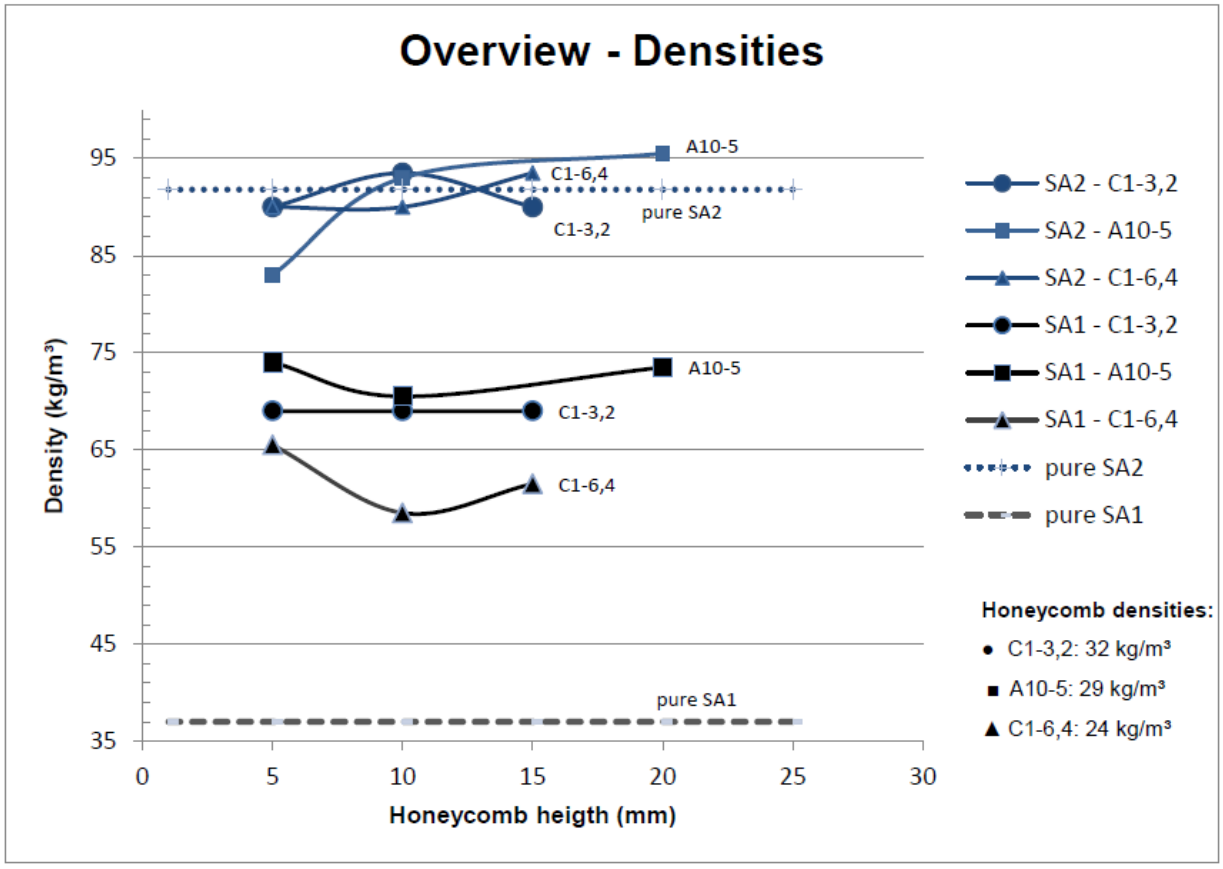


**Fig.22:** Obtained data on the samples' densities correlating to their height

Keeping a higher fault-tolerance for small heights in mind, since the measurement via hand is more inaccurate then, one can find in Fig. 22 that the densities do in fact not correlate with the height of the composite as expected. Therefore the composites' density can be taken as a constant over different heights. When looking at the data for the semi-flexible SA2 it makes sense, that the heavier aerogel with a density of 92 kg/m³ and a mass fraction of around 70% impacts the composite's weight more than the honeycomb with a weight of around 29 kg/m³. Also the data correspond to the different densities of the honeycomb: The lightest composites are the C1-6,4-based, the heaviest are the A10-5-based. When calculating the theoretical densities of the composites with the rule of mixtures, as described in II.C.iv), the data in Tab. 18 are obtained.

**Tab. 18:** Theoretical calculations of the densities of the composites in contrast to the experimental results

| Sample: | | Homeycomb ($g/cm^3$): | Aerogel ($g/cm^3$): | Theoretical density ($g/cm^3$): | Exp. density ($g/cm^3$): | Difference theory/exp.: |
|---|---|---|---|---|---|---|
| **SA1** | C1-3,2-29 | 0,029 | 0,037 | 0,036 | 0,069 | + 89 %. |
| | C1-6,4-24 | 0,024 | 0,037 | 0,036 | 0,073 | + 99 %. |
| | A10-5-32 | 0,032 | 0,037 | 0,037 | 0,062 | + 68 %. |
| **SA2** | C1-3,2-29 | 0,029 | 0,092 | 0,087 | 0,091 | + 5 %. |
| | C1-6,4-24 | 0,024 | 0,092 | 0,089 | 0,091 | + 1 %. |
| | A10-5-32 | 0,032 | 0,092 | 0,089 | 0,092 | + 3 %. |

Obviously, the theoretical values for SA1 do not match the experimental data, which is around 70-100% percent higher. This vast difference indicates a high margin of error for the only roughly estimated density of the SA1-aerogel. One reason for this error lies in the fact, that SA1's density can only be measured badly and imprecisely because of its fragility. Given that the established SA1 density is the arithmetic mean of two badly measurable SA1 reference samples, its relative error is considered high. Therefore the calculated theoretical density is inaccurate, too. Also some aerogel protrudes from the cells, which cannot be cut without damaging the aerogel structure in the honeycomb cells (Fig. 23). This disturbs the measurement as well. Altogether this accounts for difference between the experimental the theoretical results. For SA2-based composites on the other hand, the theoretical and experimental results match quite well with a margin of error of <5%. This indicates a proper

correlation between the theoretical and experimental results when using the rule of mixtures in spite of the bad values for SA1.

**Fig. 23:** SA1 composite with characteristic protruding aerogel on top, which worsens the exact measurement of height

### Composite in volume percent

The volume fraction of the aerogel, mentioned in the data sheets Tab. 11 to Tab. 17 (Data III.A) and recalled in Tab. 19, is theoretically calculated as described in section II.c.i). Apparently, the volume fraction of the aerogel fills the honeycombs over 90%. It is only dependent on the dimensions of the honeycomb used. Therefore carefully choosing the utilized honeycomb gives an opportunity to tailor the composites' characteristics.

| Cell configuration: | Aerogel vol.fraction(%): | Homeycomb vol.fraction(%): |
|---|---|---|
| C1-3,2-29 | 92,7 | 7,3 |
| C1-6,4-24 | 96,2 | 3,8 |
| A10-5-32 | 95,0 | 5,0 |

**Tab. 19:** Aerogel and honeycomb volume fraction, depending on the honeycomb cell configuration

### ii. Thermal conductivity results (Hot Disk)

In Figure 24, the results for the thermal conductivity measurements are given for each honeycomb and aerogel, plotted against the samples' height. Experience shows that a margin of error of ± 1mW/mK can be expected. However, the smaller the height, the more prone to

errors the method is. Especially the described small bending of the honeycomb for SA2 and SA3, particularly for small heights, causes a non-planar surface, which deteriorates the measurement. SA1 on the other hand is so weak that it is hard to ensure good contact between the samples, because no weight can be placed upon them. Additionally, small crazes in the semi-flexible aerogel SA2 are expected to worsen measurements for small heights, too. The reason for this is the fact that all these effects lead to an increased heat flow via convection, although the transient plane source method (TPS) is primarily based on thermal diffusion (conduction). As a result, the data for the single sample SA2-A10-5 is marked as probably defective. Anyhow, one has to bear in mind that external influences such as high atmospheric moisture might cause a larger margin of error. Measurements were done between 23.6-27.9°C and 1003-1015 bar atmospheric pressure, with humidity ranging between 43.8-67.9% over the course of experiments.

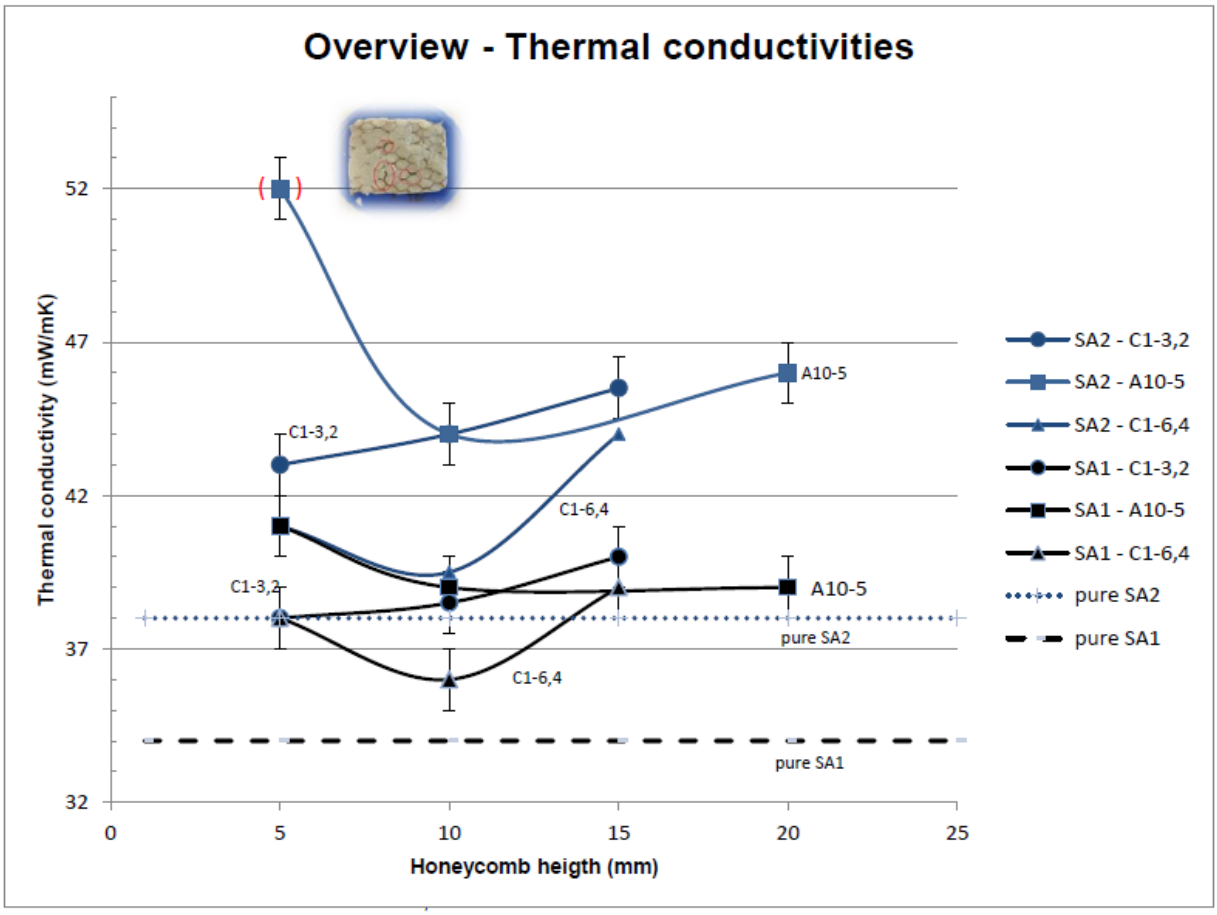


**Fig.24:** Obtained data on thermal conductivities correlating to height and cell configuration

When taking a look at the graphs in Fig. 24, the SA2-based composites are painted with blue, the SA1-based composites with black curves. The dotted lines indicate the pure aerogels' thermal conductivities (SA1 ~34 mW/mK; SA2 ~38 mW/mK). One can easily distinguish the difference of thermal conductivity the embedded aerogels cause for the composite. SA2-based composites rank on a higher level, whereas the SA1-based materials show better isolation. The minima can be found at a tallness of 10mm, except for the C1-3,2 shape. Conductivity in comparison to the honeycomb itself (60 mW/mK) was substantially decreased.

When recalling the honeycomb properties (Tab. 20), another result found is the confirmation of the assumption that the larger the cell diameter of the honeycomb is, the lower the composites' thermal conductivity is. The reason is that with a larger cell diameter, the volume and therefore the mass fraction of the isolating aerogel increases, which results in a decreased thermal conductivity for the composite.

**Tab. 20:** Recall of the properties of the utilized honeycomb, which influence the characteristics of the composite, as stated in III.A)

| Manufacturer: | Utilized honeycomb: | Cell size: | Density: | Height: | Thermal conductivity: |
|---|---|---|---|---|---|
| Schütz Industry Services | C1-3,2 | 3.2 mm | 0.029 g/cm³ | 5/10/15mm | 60 mW/mK |
| | C1-6,4 | 6.4 mm | 0.024 g/cm³ | 5/10/15mm | 60 mW/mK |
| Hexcel | A10-5 | 5 mm | 0.032 g/cm³ | 5/10/20mm | 60 mW/mK |

When calculating the theoretical thermal conductivities of the composites with the rule of mixtures, as described in II.C.iv), the data in Tab. 21 are obtained.

**Tab. 21:** Theoretical calculations of the thermal conductivities of the composites in contrast to the experimental results

| Sample: | | Therm.cond. Honeyc. (W/mK): | Therm.cond. Aeg. (W/mK): | T.c. composite in theory (W/mK): | Therm.cond. exp. (W/mK): | Difference theory/exp.: |
|---|---|---|---|---|---|---|
| SA1 | C1-3,2-29 | 0,06 | 0,034 | 0,036 | 0,038-0,040 | +5-10% |
| | C1-6,4-24 | 0,06 | 0,034 | 0,035 | 0,036-0,039 | +3-10% |
| | A10-5-32 | 0,06 | 0,034 | 0,035 | 0,039-0,041 | +10-14% |
| SA2 | C1-3,2-29 | 0,06 | 0,038 | 0,040 | 0,043-0,0455 | +7-12% |
| | C1-6,4-24 | 0,06 | 0,038 | 0,039 | 0,044-(0,052) | +11-(25)% |
| | A10-5-32 | 0,06 | 0,038 | 0,039 | 0,0395-0,044 | +1-11% |

One can see that even this simple method allows a decent appraisal of the resulting thermal conductivities: The experimental properties are about 10-15% higher than the theoretical values. This sounds reasonable concerning the previously described defects and problems with the measurement method. Therefore this approach is suited for rough approximations when designing aerogel honeycomb composite materials.

### iii. Mechanical properties

As a general rule, the quadratic specimens were compressed to 50% of the original length in-plane and out-of-plane with a compression rate of 1mm/min as described in section III.d.vi). Further discussion on mechanical testing of honeycomb is done by XY et al. [59].

#### Stress / compression

Fig. 25 & 26 display the load/displacement data of four representative samples of A10-5,2 cell configuration such as the data for aerogel reference and empty honeycomb samples. The delayed rise of the curve for the out-of-plane (oop) measurements is caused by protruding aerogel, which could not be cut perfectly without damaging the composites' structure. Therefore there is an offset. For the honeycomb the nearly linear behavior of the first part of the slope, which can be found for all samples, indicates elastic behavior over a large deformation (~17% for in-plane and ~3% for out-of-plane). The linear relation between stress and compression ends with a maximum followed by a region of almost constant pressure (plateau in the stress/compression curves).

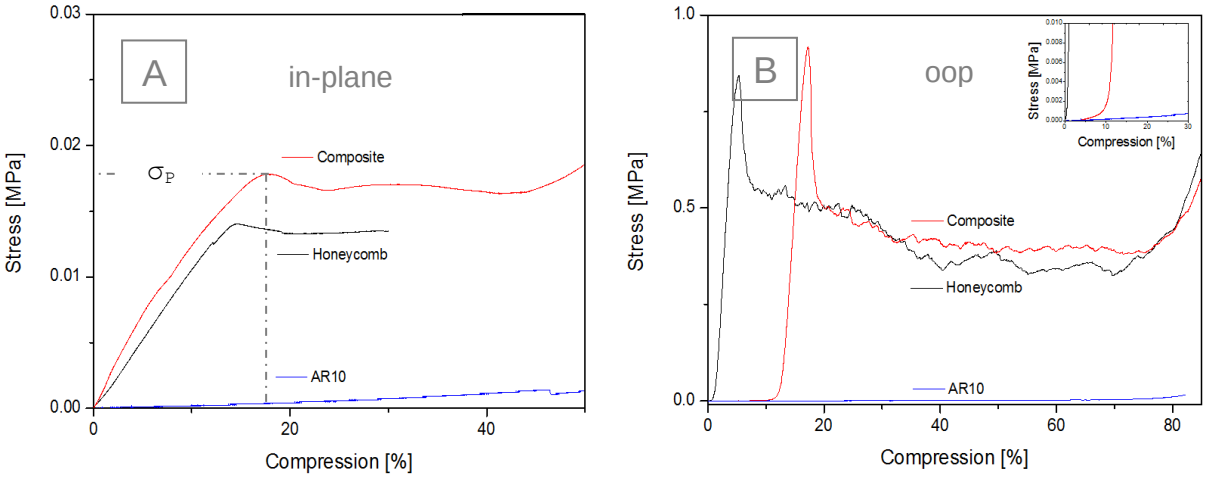


**Fig.25:** Representative obtained stress-compression curves for a super-flexible-SA1-based composite of A10-5,2 size for in-plane compression (A) such as out-of-plane compression (B)

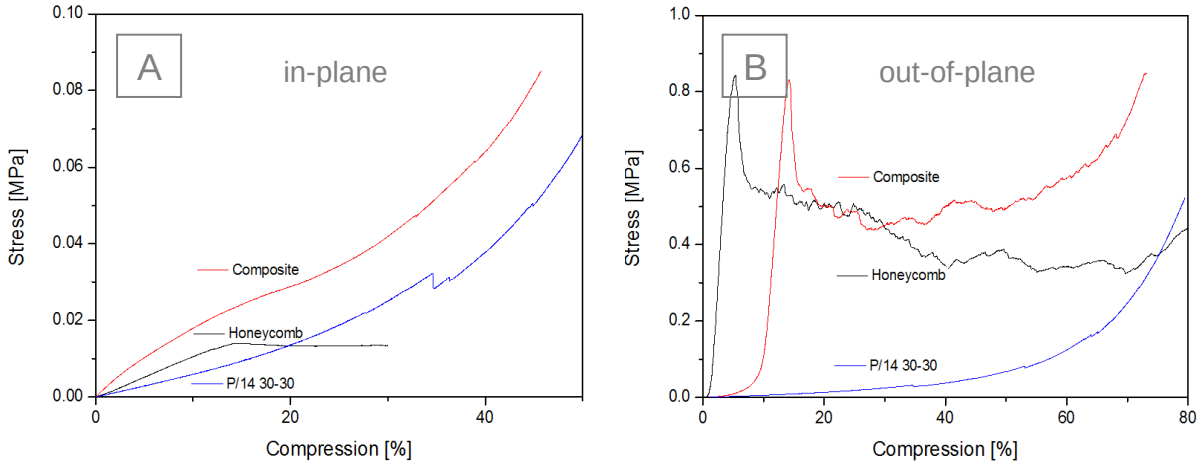


**Fig.26:** Representative obtained stress-compression curves for a semi-flexible-SA2-based composite of A10-5,2 size for in-plane compression (A) as out-of-plane compression (B)

Also the pure aerogels show a linear elastic behavior at first (SA1 until ~15%, SA2 until ~8%). Then strain hardening occurs. When analyzing the exemplary stress compression curves of the composites shown in Fig. 25 and Fig.26 qualitative, they literally behave like a combination of both the aerogels‘ and honeycomb’s stress-compression-curves. One can see that the apparent Young’s modulus such as the maximum tolerable load is increased significantly compared to the pure aerogel in both cases and that they are even higher than the honeycombs’. This proves that increased apparent Young’s moduli and bearable stresses are obtained as desired.

Additionally the peak stresses $\sigma_P$ (see Fig. 25 (A)) of the honeycombs and composites can be compared (Tab. 22 and Tab. 23).

When analyzing the data for out-of-plane compression (Tab. 22) one can see that SA1-based composites tend to have a lower $\sigma_P$ than the honeycomb. As discussed in section C.I), this can be explained with chemically weakened honeycombs. However this effect is weaker for Hexcel’s honeycombs A10-5-32. The reason for this might be the utilization of a different glue for the honeycomb bonding. The $\sigma_P$ for SA2-based composites on the other hand are slightly increased. This corresponds to the higher stiffness of SA2 aerogels, which hinders the honeycomb walls from buckling and therefore increases the observed $\sigma_P$.such as the higher level of the plateaus in Fig. 26 (B). Small negative differences can be explained by measurement inaccuracy.

| | Sample: | | $\sigma_P$ honeycomb: | $\sigma_P$ composite: | Difference: |
|---|---|---|---|---|---|
| SA1 | C1-3,2-29 | 5mm | 0,53 | - | - |
| | | 10mm | 0,48 | 0,35 | -27 %, |
| | | 15mm | 0,49 | 0,34 | -31 %, |
| | C1-6,4-24 | 5mm | 0,47 | 0,36 | -23 %, |
| | | 10mm | 0,46 | 0,42 | -9 %, |
| | | 15mm | 0,43 | 0,38 | -12 %, |
| | A10-5-32 | 5mm | 0,89 | 0,98 | + 10 %, |
| | | 10mm | 0,92 | 0,88 | -4 %, |
| | | 20mm | 0,84 | 0,91 | + 8 %, |
| SA2 | C1-3,2-29 | 5mm | 0,53 | - | - |
| | | 10mm | 0,48 | 0,570 | + 19 %, |
| | | 15mm | 0,49 | 0,590 | + 20 %, |
| | C1-6,4-24 | 5mm | 0,47 | 0,590 | + 26 %, |
| | | 10mm | 0,46 | 0,440 | -4 %, |
| | | 15mm | 0,43 | 0,450 | + 5 %, |
| | A10-5-32 | 5mm | 0,89 | 0,96 | + 8 %, |
| | | 10mm | 0,92 | 0,88 | -4 %, |
| | | 20mm | 0,84 | 0,82 | -2 %, |

**Tab. 22**: Peak stresses $\sigma_P$ for out-of-plane compression of SA1- and SA2-based composites compared to their honeycomb reference samples

When having a look at the results from in-plane compression the peak stresses $\sigma_P$ show significant differences (Tab. 23). This can be explained by a high margin of error, because the non-stabilized honeycombs tend to bend when tested as seen in Fig. 27.

| | Sample: | | $\sigma_p$ honeycomb: | $\sigma_p$ composite: | Difference: |
|---|---|---|---|---|---|
| SA1 | C1-3,2-29 | 5mm | 0,01 | - | - |
| | | 10mm | 0,0094 | 0,0067 | -29 %, |
| | | 15mm | 0,0133 | 0,0056 | -58 %, |
| | C1-6,4-24 | 5mm | 0,0042 | 0,004 | -5 %, |
| | | 10mm | 0,006 | 0,005 | -17 %, |
| | | 15mm | 0,006 | 0,007 | 17 %, |
| | A10-5-32 | 5mm | 0,005 | 0,011 | 120 %, |
| | | 10mm | 0,004 | 0,011 | 175 %, |
| | | 20mm | 0,005 | 0,018 | 260 %, |

**Tab. 23**: Peak stresses $\sigma_P$ for in-plane compression

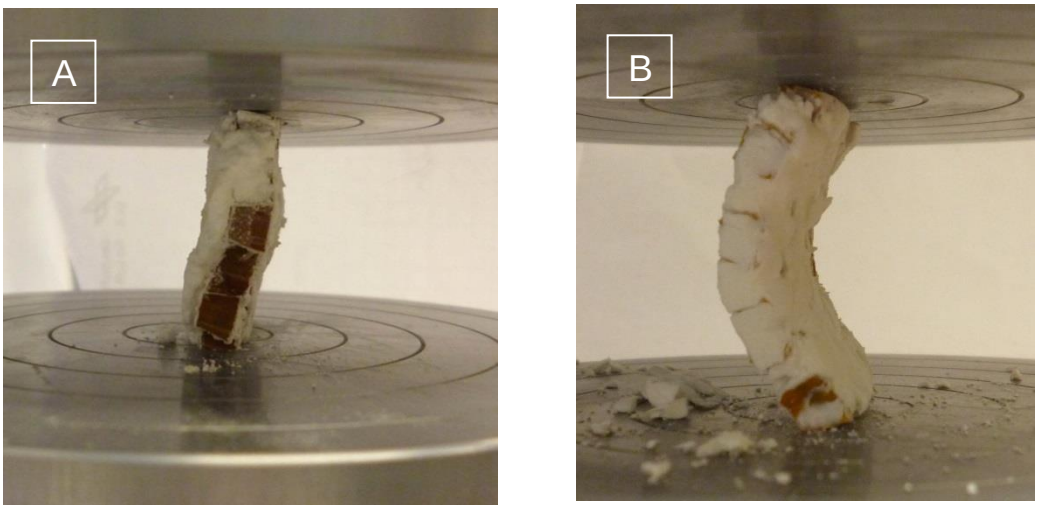


**Fig. 27**: Bending of non-stabilized honeycomb-based composites for in-plane compression (A: SA1 C1-6,4-5mm 15% deformation; B: SA2 A10-3,2-5mm 15% deformation)

Fig. 26 (A) shows, that for in-plane compression of SA2-based composites no specific peak stress can be measured. Therefore the difference of the composite's and the honeycomb's bearable stresses at similar deformation $\Delta\sigma$ is introduced. This value can indicate an increase

or decrease of mechanical stability of the composite compared to the pure honeycomb. Tab. 24 shows the obtained $\Delta\sigma$ for in-plane compression of SA2-based composites.

| | Sample: | | σ honeycomb: | σ SA2-composite: | Difference Δσ: |
|---|---|---|---|---|---|
| SA2 | C1-3,2-29 | 5mm | - | 0,01 | - |
| | | 10mm | 0,006 | 0,027 | +350,0 % |
| | | 15mm | 0,006 | 0,019 | +216,7 % |
| | C1-6,4-24 | 5mm | 0,005 | 0,006 | +20,0 % |
| | | 10mm | 0,004 | 0,012 | +200,0 % |
| | | 15mm | 0,005 | 0,026 | +420,0 % |
| | A10-5-32 | 5mm | 0,01 | - | - |
| | | 10mm | 0,0094 | 0,021 | +123,4 % |
| | | 20mm | 0,0133 | 0,023 | +72,9 % |

**Tab. 24**: Difference $\Delta\sigma$ between the stress level of the SA2-composite and a honeycomb reference sample at the buckling point of the honeycomb for in-plane compression

The difference can be explained via the measurement method: At first the empty honeycomb's buckling stress and the associated compression is measured. Then the bearable stress of the composite at this specific compression is compared. However this point does not match with the aerogels peak stress. For all samples except the C1-6,4-24mm, this point already is within the area of densification.

The SA1-based composites show apparent Young's moduli defined by the honeycombs' moduli, as seen in Fig. 28 and Fig. 29. Slightly higher bearable stresses indicate some, even though small, influence of the added super-flexible aerogel. This is also reflected by a longer interval of quasi-linear elastic deformability, seen in Fig. 25.
Also the SA2-based composites show honeycomb-driven properties at the beginning (Fig.27). Especially when testing the in-plane-direction. At about one third of the plotted compression-scale, around 15% for ip and 35% for oop, the effect of the embedded aerogel becomes noticeable compared to the pure honeycomb curve. At this stage, the already compressed aerogel begins to hinder further compression more and more where empty cells would not.

### Experimental apparent Young's moduli in the composite

With the stress/compression curves of all samples, both in-plane and out-of-plane apparent Young's moduli could be determined from the initial slope of the curves for all recipes and honeycomb sizes. Fig. 28-31 below show the results.

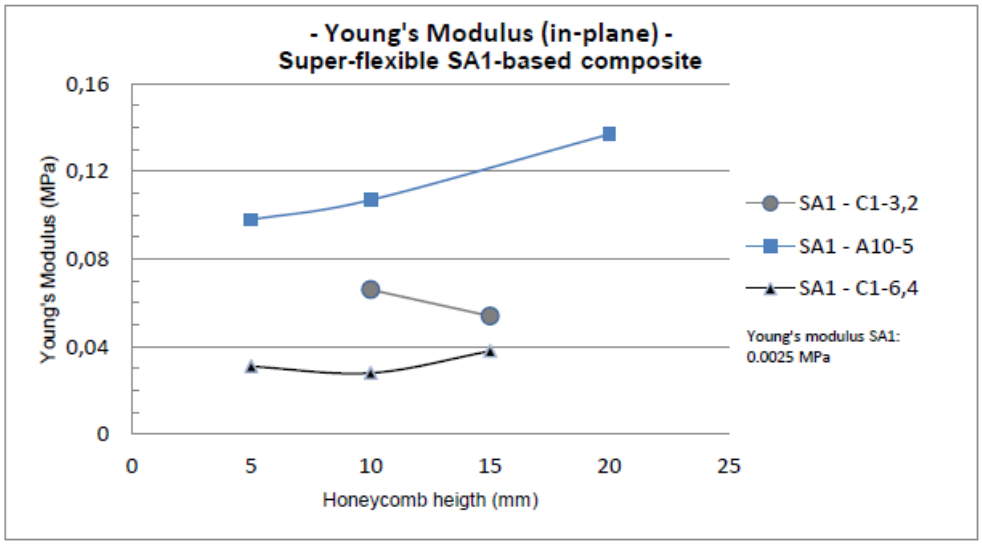


**Fig.28:** Apparent Young's modulus of super-flexible SA1-based composites in-plane

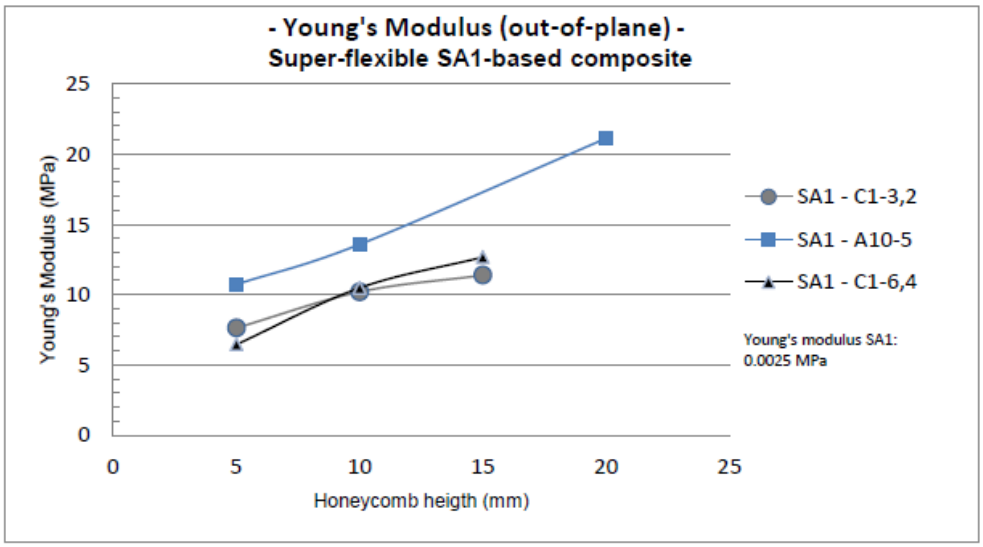


**Fig.29:** Apparent Young's modulus of super-flexible SA1-based composites out-of-plane

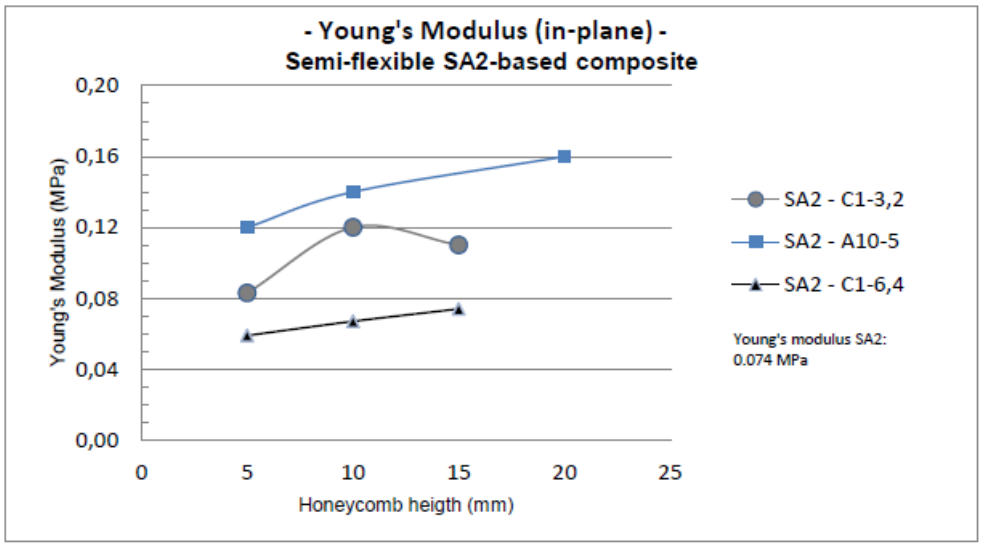


**Fig.30:** Apparent Young's modulus of semi-flexible SA2-based composites in-plane

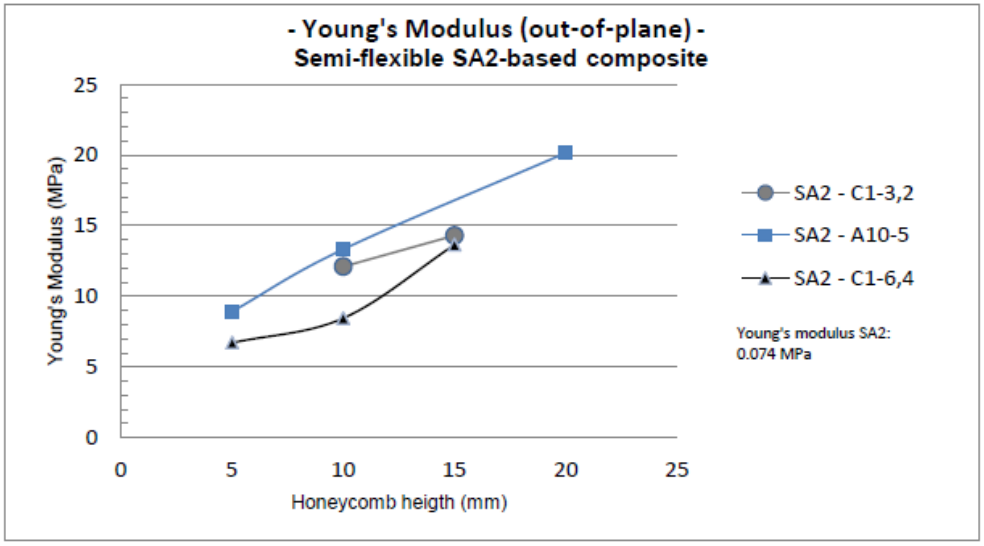


**Fig.31:** Apparent Young's modulus of semi-flexible SA2-based composites out-of-plane

The graphs show the correlation between the sample height and its apparent Young's modulus for each honeycomb shape. The most striking result for all samples is the increase of the Young's modulus with increasing sample height. This effect is quite significant. On its maximum, detected for a 20mm SA2-A10-5 sample, seen in Fig.31,

the apparent modulus is twice as high as for its 5mm high counterpart. The reasons for this are the honeycombs themselves. When looking at the apparent Young's moduli of the honeycombs (Fig. 32), they are accountable for the increases seen in Fig. 27-31.

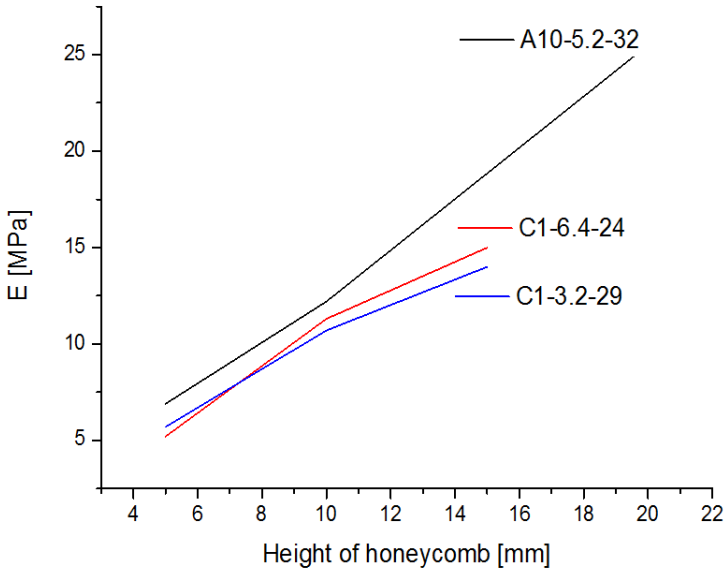


**Fig. 32:** Increase of the apparent Young's modulus of different honeycombs with height

### General remarks - weakening of the honeycomb bonding

When investigating compressed samples of SA1-based composites after the mechanical testing, the bonding via the adhesive surface of some of the honeycomb cells was torn apart (see Fig. 33). This indicates a weakening of the aramid-structure during synthesis. An explanation for this discovery is exhibited in IV.C).

**Fig.33:** Image of a compressed SA1-based composite sample, showing damaged linking

### iv. SEM analysis

SEM analysis was used to gain insight into the nano-structure of the aerogel such as the adhesion between honeycomb and aerogel. For that purpose, images of the reference samples consisting of pure aerogel on the one hand and the composite samples on the other hand were taken. In this section, these images are discussed.

#### SA1

First of all, the super-flexible aerogel named SA1 is inspected. Fig. 34 and Fig. 35 show SA1 in different magnification, at first with and then without honeycomb. From Fig. 34, showing the aerogel's nano-structure, the size of the particles can be assumed with approximately 1µm and tends to be homogenous. In contrast, pores with highly in homogenous pore sizes around 1-50 µm can be found.

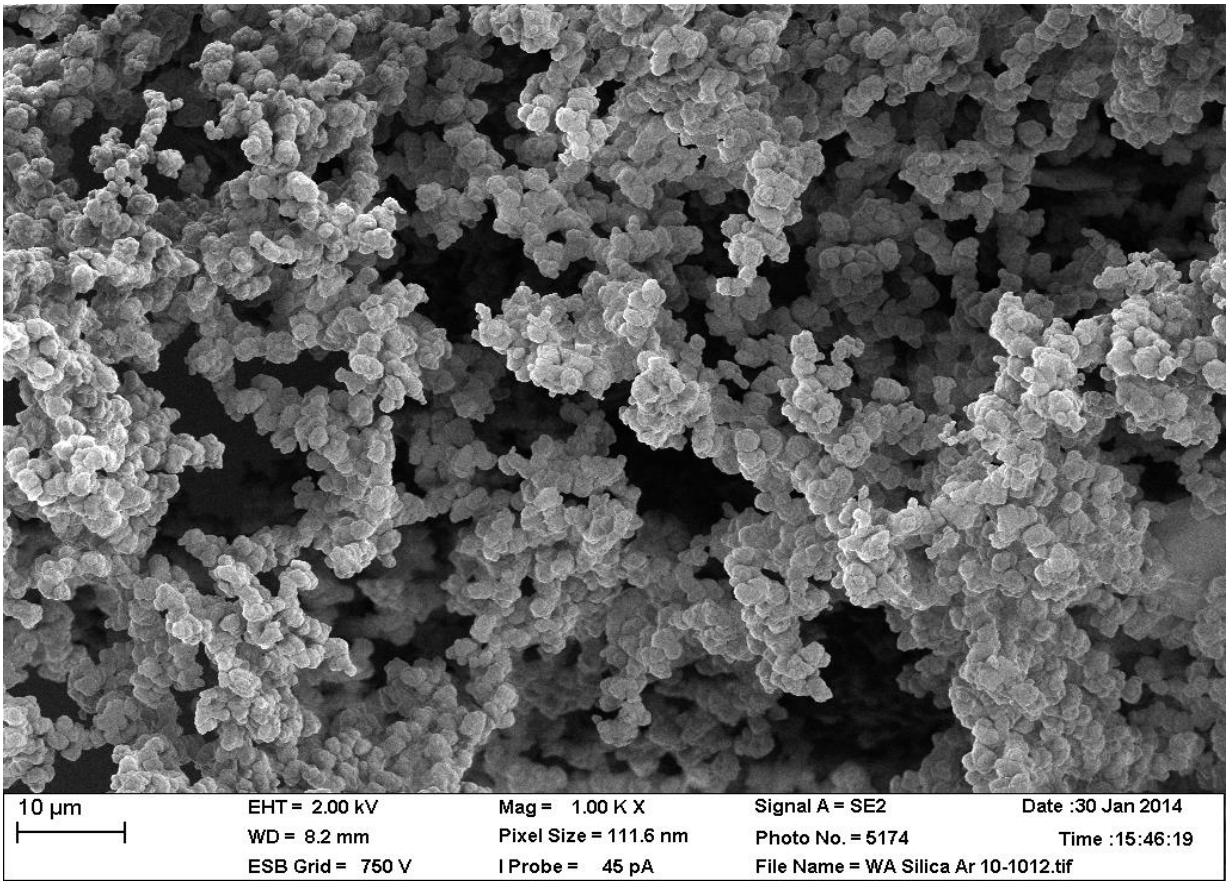


**Fig. 34:** pure SA1-aerogel 1000x enlarged, showing homogenous grainy particles and meso to macro scale pores

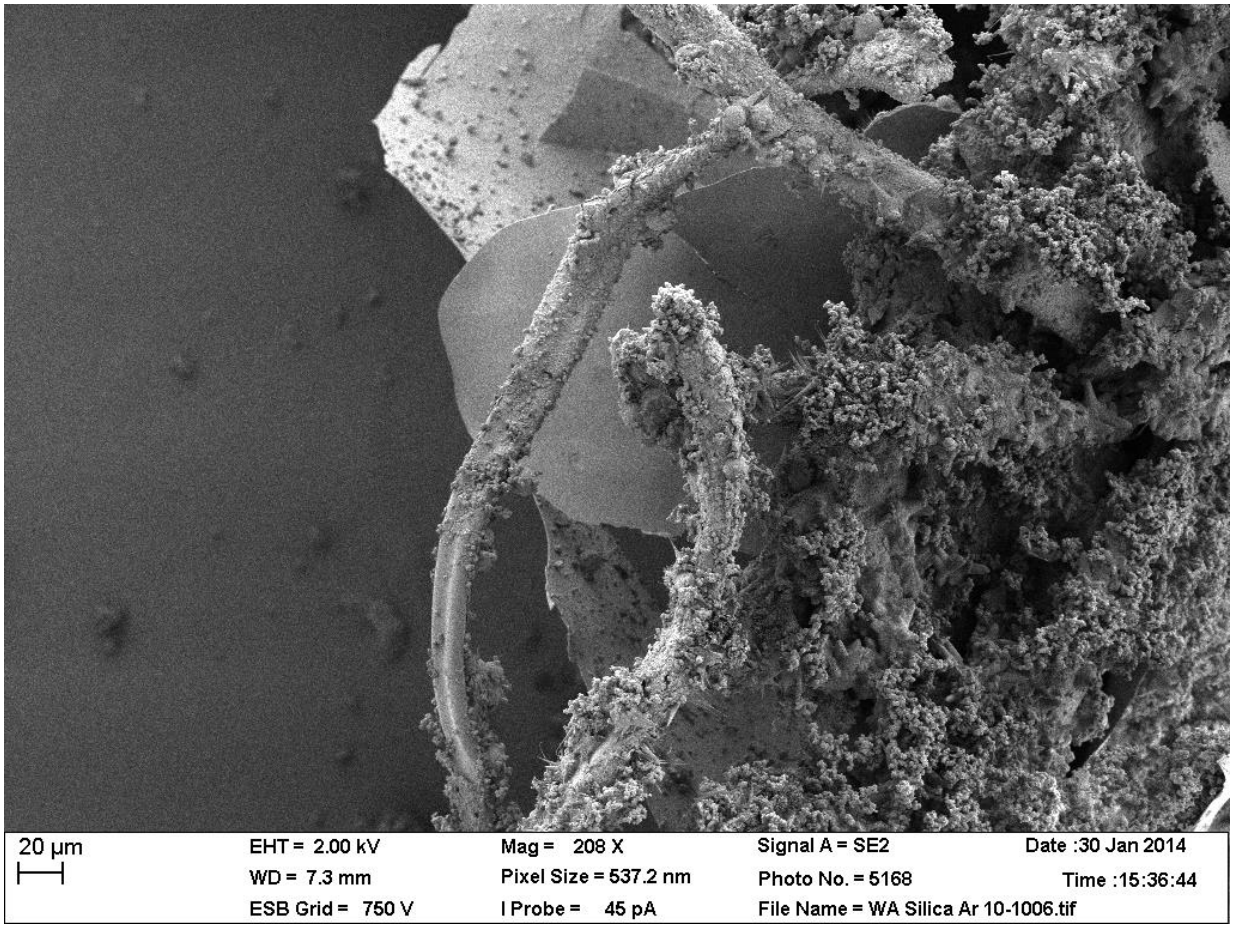


**Fig. 35:** cut off piece of SA1-aerogel-honeycomb-composite, 208x enlarged, showing aramid-fibers, covered with good adhering aerogel particles

Fig. 34 on the other hands shows a cut off piece of a composite sample. It is easy to distinguish the aerogel-covered aramid-fibers in the foreground, protruding from the cutting site. The honeycomb surface is extensively and equally covered with the aerogel shown in Fig. 35. Evidently a good adhesion between the two composite materials prevails.

### SA2

The pure flexible SA2-aerogel, photographed in Fig. 36, shows much smaller particles (less than 100 nm) than the super-flexible SA1. Significantly different pore sizes from micro to macro size can be found.

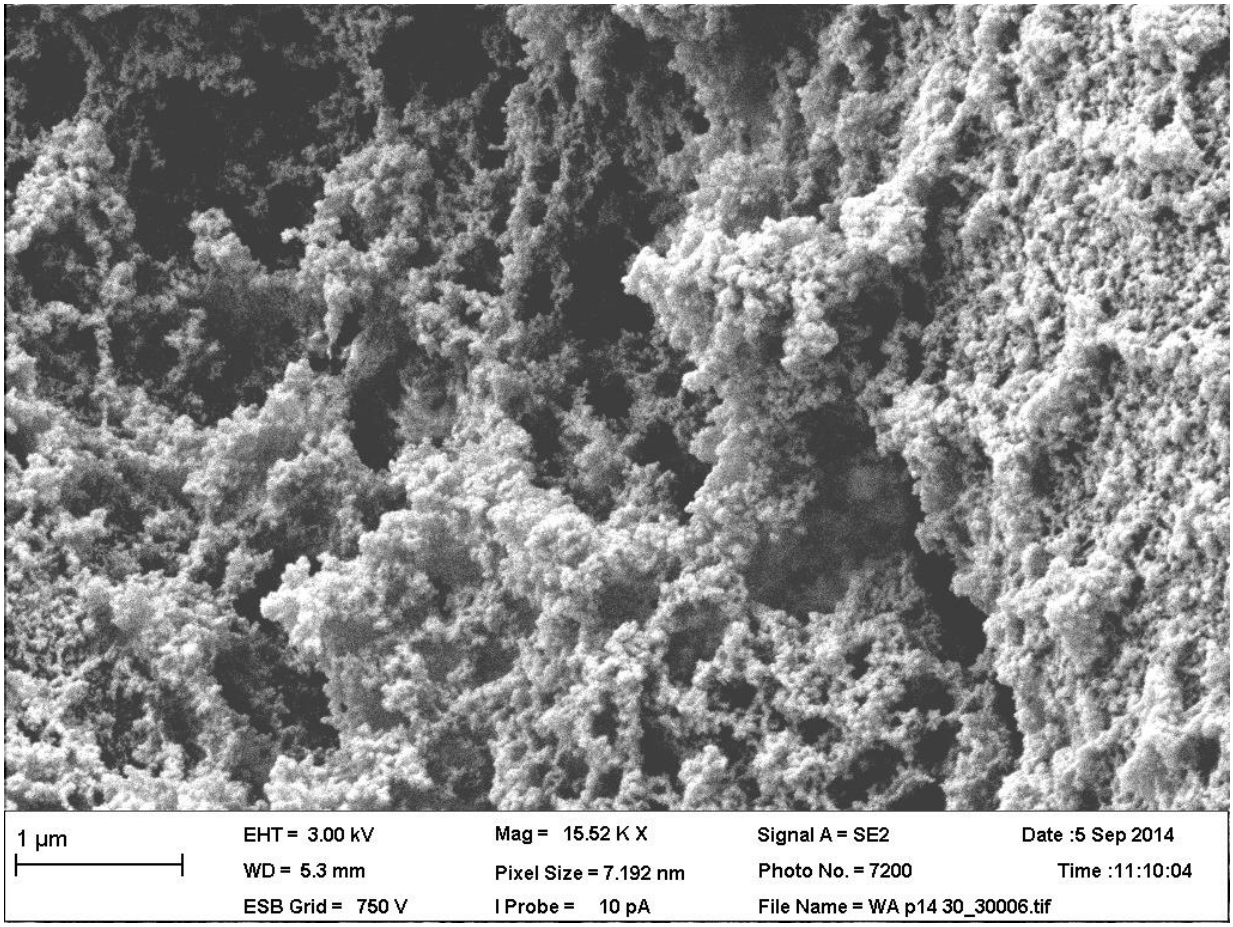


**Fig. 36:** Image of pure flexible SA2-aerogel, showing less than 100 nm large homogenous particles with enormously different pore sizes

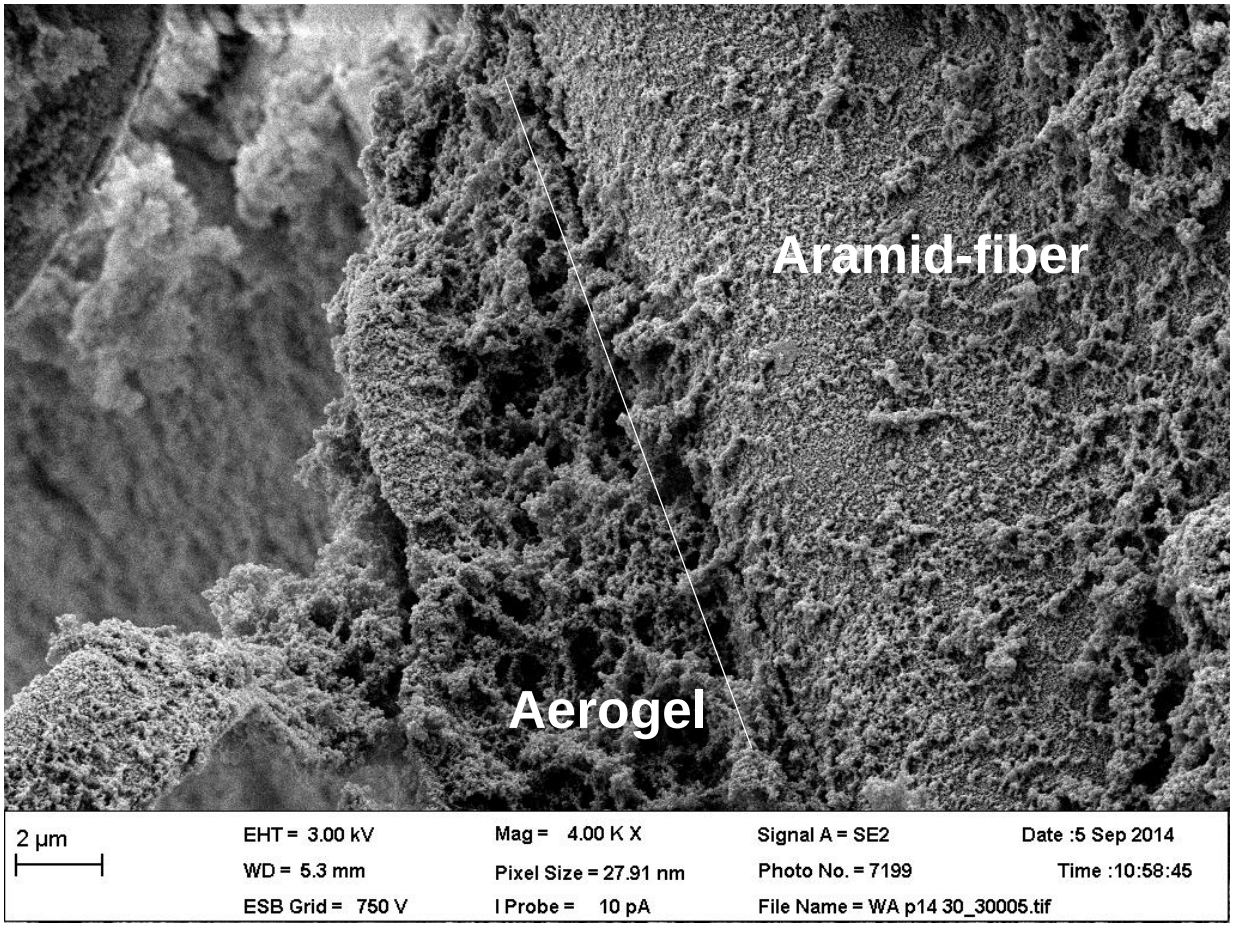


**Fig. 37:** Image of an aramid fiber, covered with flexible SA2-aerogel, indicating good adhesion

In the composite, the supporting structure of the aramid honeycomb provides a vastly increased resistance against mechanical stress of the composite in comparison to the pure aerogel. The notably good macroscopic adhesion of the SA2 aerogel on the honeycomb can now be investigated on micro level. As seen in Fig. 37, the aramid fiber is covered evenly and entirely with aerogel particles. In fact the adhesion is that good that a 6-8µm thick layer of aerogel can easily maintain the linking though suffering substantial mechanical stresses while cutting.

In comparison to the SA1 composite, the SA2 shows much smaller particles with considerably better adhesion, while maintaining a similar nano-porous structure with different pore sizes but homogenously sized particles.

### SA3

When investigating SA3-based composite via SEM, one can quickly point out the reason why the SA3 recipe was dropped for further testing: Missing adhesion between the aerogel and the honeycomb.

As seen in Fig. 38 and 39, only patches of the aramid paper are covered with small aerogel particles. Good adhesion, as seen before at SA1- or SA2-based composites, is non-existent with SA3. Despite the good thermal parameters of the recipe, this prevents further research in the context of this work.

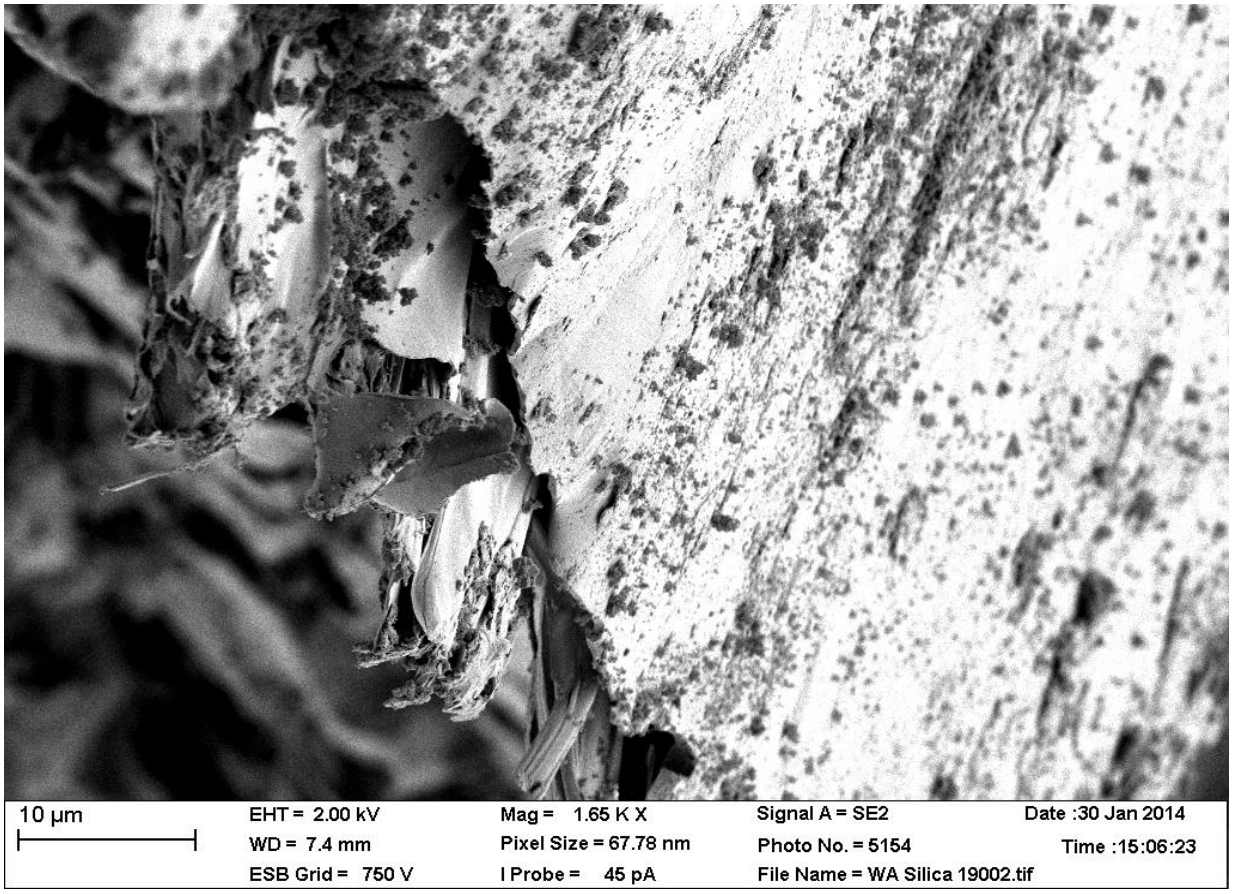


Fig. 38: Image of a cut-off piece of a SA3 aerogel composite, showing only bad aerogel adhesion on the honeycomb plane

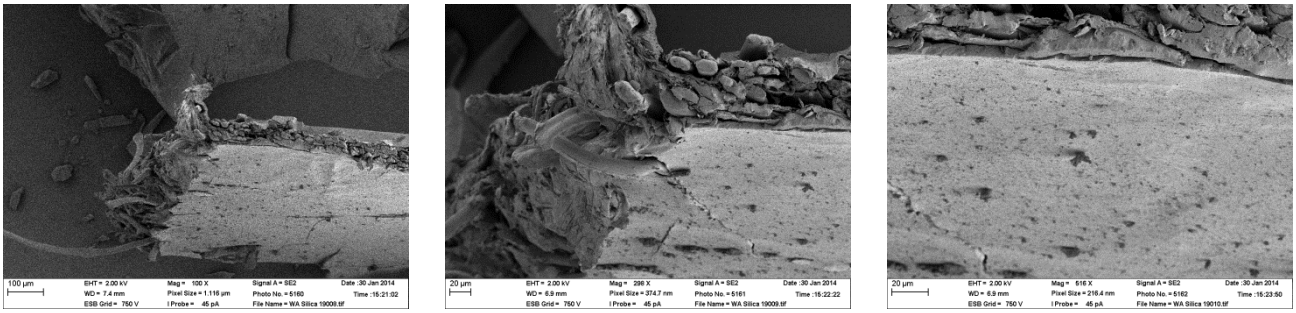

Fig. 39: Zooming in to a cut of piece of SA3-composite material from 100x to 516x, depicting the lack of adhesion

### v. Specific surface area (BET) of the utilized aerogels

BET analysis has been performed for all recipes, namely SA1, SA2 and SA3. The data of the adsorption desorption isotherms of SA1 and SA3 are plotted in Fig. 40 to Fig. 41. Due to identical synthesis and processing, a single gauging was carried out for each recipe, which is representative for all samples of that type.

For SA1, a surface area of 435.64±1 m²/g was measured. For SA2, a surface area of 359.43±1 m²/g was measured. SA3 on the other hand provides 892.08±1 m²/g of surface area for the “50+”-series, and even greater 1028.66±1 m²/g for the „fast wash“-series.

All adsorption desorption isotherms show the expected behavior. Only the SA1 desorption isotherms show an abnormal behavior on multiple measurements (Fig. 40): The large deviation of the isotherm such as the abrupt end on a higher nitrogen level than at the beginning of the measurement. This is evidence that some pores might be damaged in the process of adsorption. This is plausible with respect to the extremely fragile, almost powder-like structure of the SA1 aerogel.

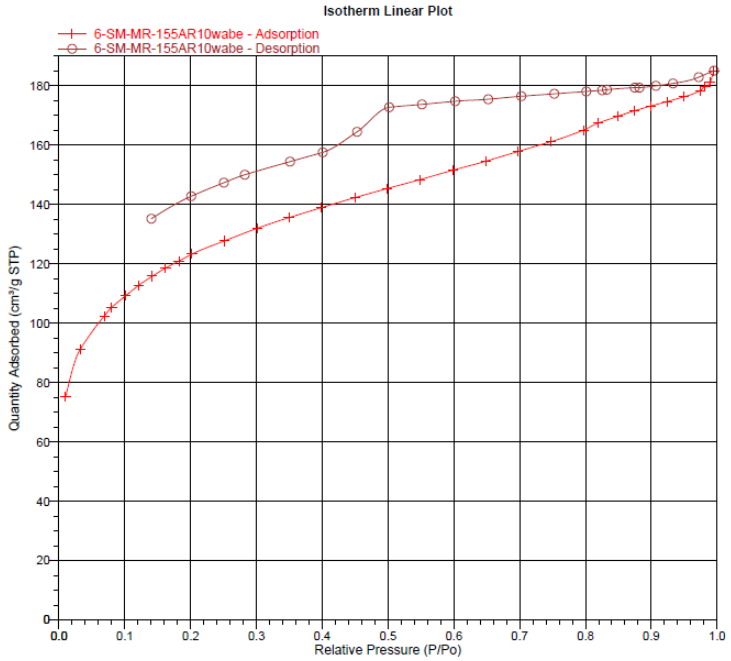


**Fig. 40:** SA1's adsorption desorption isotherms, indicating a damaged micro-porous structure

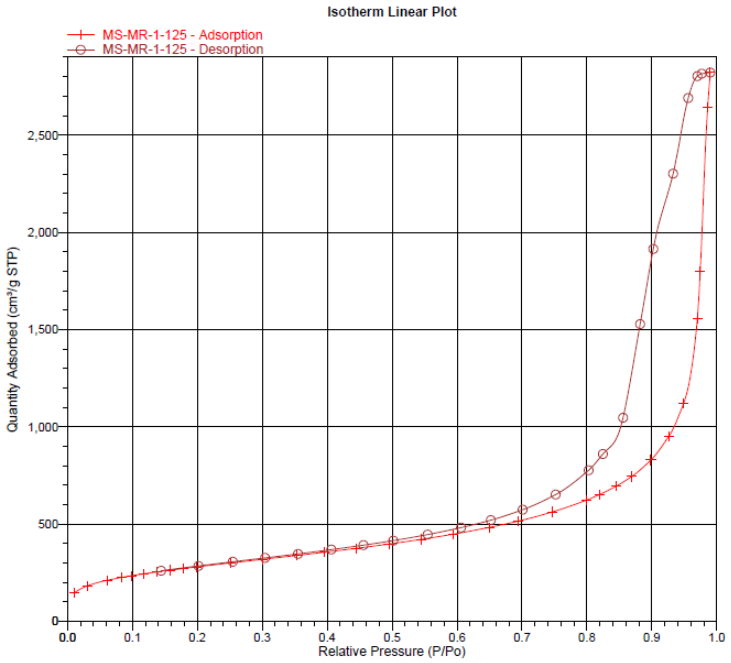


**Fig. 41:** SA3's („slowfast"-series) isotherms, indicating a proper BET measurement

# C. Conclusions

## i. Assessment of the results

First of all it was possible to synthesize composites with the aerogels SA1 and SA2 in combination with the honeycomb. SA3 showed bad adherence and too much shrinkage, which was the reason why it was discontinued. Fundaments of this work were the presented recipes, with which aerogel monoliths reference samples could be synthesized without problems. The challenges lay in the implementation of the reinforcing honeycomb. To reach that goal there will be a description of the experiences with the production process initially. Subsequent there will be a description of the perceptions concerning the honeycombs and aerogels, which will allow an evaluation of the different synthesis routes and recipes for the composites.

### *Processing in general*

#### Upscaling

Preliminary tests with pure aerogels worked without complications. Nevertheless it was necessary to enlarge the amount of sol (~ 600 ml) compared to earlier tests (ca. 20 ml) due to the higher amount of samples. The upscaling affects the synthesis, which might make an adjustment of the stirring and aging time necessary. Yet adjustments were not made in this work as the results were satisfying and an estimation of the changed properties would have been too time-consuming. For possible future applications this aspect should still be considered.

#### Washing

One rudimental weakness of the production is the pedestrian washing process. As described in the experimental section especially the flexible aerogels are very sensitive and require a lot of caution. Often samples get damaged during the decanting into the washing beakers and are not eligible for further testing, what causes a drawback for the test series. This sensitivity impedes the processing of high masses crucially, especially due to the needed careful and time consuming washing process, which takes up to 50 % of the process time. As the quality of the washing is only determined by experience this procedure has to be optimized. Big samples (e.g. 15 mm) may be washed too shortly, whereas small samples may be washed too long. Furthermore substances, which may have been solved via the cutting sites of the honeycombs during the synthesis, may require an intensified washing. E.g. SA1-composites

cause a noticeable green turning of the solvent (see next sub-section), what may be an indicator for a required conformation of the washing in order to get rid of contaminations, which may lead to a change of properties for the aerogel. After all this part of the production process may be optimized in many ways (e.g. pH-testing) and should be part of future investigations.

### *Assessment of the aerogels*

The fundaments for the manufacturing of the presented composites were three different silica-aerogels, from highly flexible to stiff. The aim was not only to synthesis the composites but also to evaluate influences of the different flexibilities of the aerogels in the process. Each of aerogels, which are well known to the working group, could be easily manufactured to monoliths without honeycomb, which makes a discussion of the single aerogels superfluous.

#### Key factor aerogel-shrinkage

However, the results in the previous section IV.B showed quite insistently that a single factor is most crucial when it comes to combining aerogels with other materials: The aerogel shrinkage. Not only can the shrinkage damage the aerogels structures itself. Also the induced tensions can give rise to other negative consequences, like deformation of the honeycomb in the composite, as found in the case of SA2-based composites. A high shrinkage foremost motivates the separation between the synthesized aerogel and the honeycomb wall, possibly resulting in cracks and bad adherence, as found for SA3-based composites. When the adherence between aerogel and honeycomb is bad, low shrinkage is a key factor in increasing the interface compatibility between the composite materials and therefore seems to be very important in controlling the fabrication of aerogel composites. Thus it is also important that the honeycomb is not weakened when it has to withstand these stresses. Unfortunately, such an effect occurs, as described in the next subsection. In this context the following observation was made by chance: After the SA3 had initially been supercritically dried in ethanol the solvent had to be changed to less polar acetone due to supply difficulties. The results showed significantly less shrinkage and cracks, which led to the fact that from this point on acetone was used for further drying. The influence of different solvents to the shrinkage of the aerogels could not be analyzed in this work, but is relevant to the described effect and should be investigated.

However, the water fraction in any utilized solvent should be minimized in any case, because water is not miscible in the supercritical $CO_2$. Therefore the pure acetone is better miscible and might be more suitable for drying than ethanol, which still contains 4% contaminants like water. Another possible effect explaining this correlation of shrinkage and solvent is presented in the following.

*Assessment of the honeycomb*

When it comes to the evaluation of honeycomb as a composite-partner for the used aerogels, a positive conclusion can be drawn. The previously described results indicate a significant increase of the mechanical stability of the composites in contrast to the pure aerogels (IV.B), which was the objective of the implementation of the honeycombs. For example samples of SA2-composite, whose reference samples broke while handling due to instability, emerged as being significantly more resistant. Especially SA1 is difficult to use without a reinforcing structure due to its superflexibility.

But irrespective of their merits the honeycombs themselves were enervated by the manufacturing process. Some of them were deformed or shrank as described in section IV.B. Others showed weakened torn-apart bondings after mechanical testing, which indicate some kind of chemical weakening. Considerations about this are discussed hereafter.

Assumption of honeycomb deformation correlating to solvent soak up and polarity

A possible explanation for different shrank results of the SA3 test series could be the following:

A contraction in H-direction was observed. The honeycomb was built from Nomex paper, which consists out of aramid fiber. In the production, various layers of paper are placed one above another in wet state and are “tilted up” into H-direction to form honeycombs. Afterwards they are dried in this shape. During the carried out synthesis and drying, ethanol can diffuse via the interface into the honeycomb over a long period of 2-3 weeks, partly at 50°C and increased compression during supercritical drying. Thereby, the moisture soaking aramid is getting „wet as in the production process“. According to the producer, in this condition the aramid papers strive back to their initial layer state. Thus, the honeycombs lose their shape to some extent due to relaxation, which looks like a contraction in H-direction. But then this contraction has to lead to tension or motion in the composite which will have to be compensated by the aerogel in the end. Tests with honeycomb submerged into ethanol for

multiple weeks (i.e. 3+ weeks like in the manufacturing process) confirms this thesis, that this “soaking up” leads to the deformation of the honeycomb.

Also important is the fact, that the lower the aerogels flexibility the higher the chance is to be damaged through the tension occurring in the honeycomb. This covers the results found and shows that also a possible „motion“ of the honeycomb during the production of composites has to be considered. If it is now assumed that the more polar ethanol weakened the aramid honeycombs under increased temperature and pressure, better results are explained for the supercritical drying in acetone as follows: In comparison to ethanol, acetone is less polar and is less absorbed by the honeycomb. Therefore the aramid paper is moistening slower and less intensive. The consequence is less relaxation to paper sheet form so that less deformed and correspondingly more monolithic composites are obtained after the process.

### Bonding ruptures due to chemical weakening of the aramid honeycomb

Furthermore a rip-off of the honeycomb bonding had been observed during the compression test, which had not been observed with pure honeycombs. During the compression test the bonding of the single aramid-paper layers tore apart in some samples due to the charged stress. An example for this observance is showcased in Fig. 42 and 43. The rips seem to start on the edging and move to the center of the sample according to the basic theory of crack propagation [60]. Some samples show this effect for in-plane stress as well.

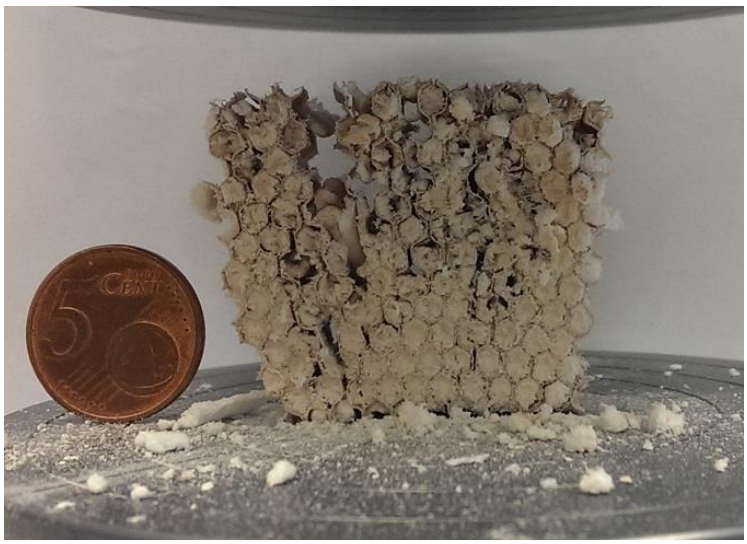

**Fig. 42:** Picture of a composite, consisting of SA1 and C1-3,2-15mm-honeycomb, after in-plane compression, showing a rupture along the honeycomb bonding

**Fig. 43:** Picture of a composite, consisting of SA1 and C1-3,2-10mm-honeycomb, after out-of-plane compression

An explanation of this phenomenon is the following assumption: Since the honeycombs are submerged in polar ethanol for a long time during synthesis this will lead to a partial dissolution of the glue used. This reaction can be further promoted by basic conditions. This accounts for the previously described green color in the alkaline catalyzed SA1 synthesis.

### Assumption of better adhesion of SA2-based composites

So when the solvent used in the aerogel synthesis seeps into the aramid paper, it is weakened as previously described. The usage of GPTMS in the synthesis of SA2 leads to the formation of polar groups which ensure additional hydrogen bonds to both phenolic resin and aramid which in return improved the contact between the materials.

*Assessment of the composites:*

### SA1:

SA1 can be basically rated as suitable for the synthesis of aramid honeycomb reinforced composites. However it is not promising for larger series. In fact, acceptable thermal

conductivities around 0.036-0.041 W/mK were found, which represents an ~10-15% increase in conductivity, compared to the pure aerogel, with a honeycomb dominated apparent Young's moduli of up to 0.137 MPa in-plane / 21.13 MPA out-of-plane. Nevertheless the production process (with five days of aging and high fragility of the alcogels) is very protracted and prone to failure. Noticeable is the described weakening of the honeycomb structure through amine-groups, which was caused by the strongly alkaline sol at the beginning of the process. This process, which is especially relevant with larger probes, requires further examination, not only concerning the impairment of the honeycomb, but also concerning its consequences for the structure of the aerogel. Also problematical is the washing and supercritical drying of the fragile aerogel composites. Elaborate washing, i.e. exchanging solvent with a pipette in the beakers, and also supercritical drying of the probes in their beakers, covered with paper is, is an extensive process, which is not suitable for large scale applications. Once the composite is produced, the previously described bad adhesion discovered via SEM cannot be perceived negative macroscopically. If it is possible to conceal the dusty aerogel in the honeycomb, the composite based on SA1 could definitely develop potential (see exemplary foil-clad SA3 honeycomb Fig. 44).

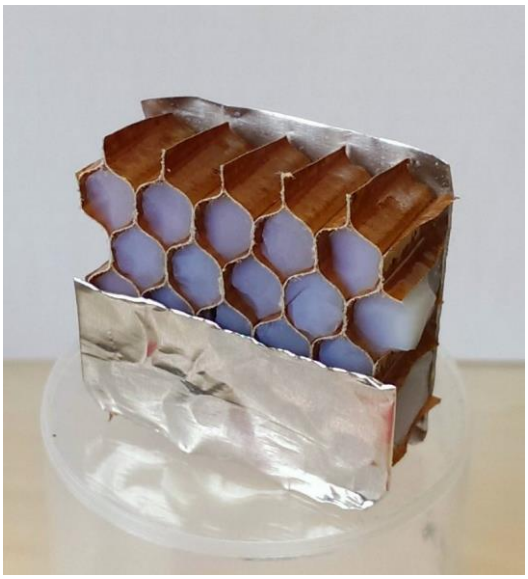

**Fig. 44:** Picture of a foil-clad SA3-based composite, showing exemplarily concealing of aerogels

SA2:

The synthesized silica aerogel was well connected to the surface of the honeycomb, showing good interface compatibility without any major defects, but only rare crazes (Fig. 45). It has potential in any account. The alcogel is also sensitive, especially during the washing. However after the supercritical drying it makes the best impression of all tested aerogel composites when it comes to overall appearance. The good monolithic structure of the composites showed acceptable thermal conductivities and above all good honeycomb-caused mechanical properties, which significantly outreached those of the aerogels in the pure honeycomb.

**Fig. 45:** Picture of a respectable SA2-based composite, considerable for further applications

SA3

Figure 46 shows the macroscopic appearance of the inflexible silica aerogel in a C1-3,2-10mm honeycomb structure after supercritical drying.

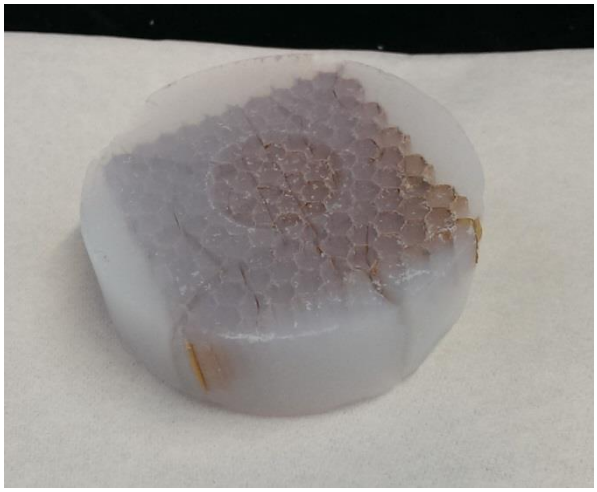

**Fig. 46:** Picture of a notably monolithic SA3-based composite, still showing major cracks

Though one of the most monolithic samples obtained, it still suffers from major cracks, making a thermal conductivity measurement obsolete. The inflexibility makes the composite susceptible for occurring stresses during fabrication, which are damaging its structure. Emerged cracks do not only prohibit an effective thermal insulation, but are a possible predetermined breaking point. Furthermore, the bad adherence between the honeycomb and the filling aerogel is an issue. In combination, these two effects lead to the conclusion, that this aerogel is obviously not practical for the synthesis of an aramid-honeycomb reinforced silica aerogel composite.

### ii. Deduced key factors for successful fabrication

In conclusion, the key factors for a successful aerogel-aramid-honeycomb fabrication can be pointed out as follows:

#### Finding a suitable aerogel

- with low shrinkage
  - ➔ otherwise the aerogel withdraws from the honeycomb cell wall, weakening adhesion between the composite materials
  - ➔ otherwise arising inner stresses can cause bending and deformation of the honeycomb

- with sufficient flexibility to withstand minor stresses and deformation during fabrication
- with sufficient mechanical stability in alcogel and aerogel form to allow proper handling and treatment without particular caution, especially for large scale manufacturing and application
- good adherence to honeycomb wall

### Proper handling of the honeycomb

- Prevent deformation:
  - Prevent honeycomb constriction, caused by solvents of aqueous environments, which drip into the aramid paper via uncoated cuts, with:
    - a new coating of already cut honeycomb parts
    - usage of less polar solvents for washing and therefore reducing effects of soaking
  - Prevent deformation, caused by significantly shrinking aerogels (as seen with SA2, shrinking about 15%)
  - Consider inner tensions, arising from different coefficient of thermal expansion of honeycomb and phenol resin at high temperature applications

All in all it is therefore not only relevant that the utilized aerogels are synthesized shrinkage-free, but also important to consider the honeycombs' behavior in the manufacturing process.

### Ensuring adherence between aerogel and honeycomb

From the experiences with the shrinkage of aerogel and honeycomb one can conclude, that good adhesion between the two composite materials is crucial. Given good adherence, the stresses occurring will not necessarily lead to cracks between the two materials and therefore the loss of the composite element can be prevented. Additionally, good adherence accounts for improved mechanical properties. To improve adhesion an adhesion-promoting surface coating is a promising option.

Proper processing

- Adjusting synthesis when upscaling
- Ensuring efficient but sufficient washing of the composite to remove perturbing dissolved compounds from the honeycomb
- Operate aging in a way that air bubbles, possibly leaking from the honeycomb when heated, can escape before the aerogel nano-structure has fully arranged and gas bubbles get caged between the structure and the cell walls, worsening thermal and mechanical properties
- Arrange handling routine for the samples, which reduces the chance of damaging the fragile samples while processing

When these key factors are paid attention to, aramid-honeycomb reinforced aerogel composites can be manufactured.

# V. Résumé and outlook

In this thesis three different nano-porous silica aerogels are embedded in mechanically reinforcing aramid honeycomb structures of different dimensions, which drastically improved their apparent Young's modulus in the magnitude of >1000 for SA1-based composites and in the magnitude of >100 for SA2-based composites for out-of-plane compression. They were prepared by employing a two-step acid–base sol–gel process utilizing the silicon alkoxides methyltrimethoxysilane (MTMS) or tetraethylorthosilicate (TEOS) as precursors and supercritically dried in $CO_2$. The results confirm the assumption that the aramid honeycombs have a minor effect on the thermal conductivities of the composites (only ~10-15% increase in comparison the pure aerogels), though the mechanical properties are increased significantly. When paying attention to the deduced key factors of fabrication, the concept of aramid honeycomb reinforced aerogel composites can be further improved. Hence it was demonstrated that aerogel-honeycomb composite materials yield potential to enable new practical applications for silica aerogel materials via diminishing their limiting fragility.

# VI. References

[1] Hosseinali Omranpour, Siamak Motahari, J. Non-Cryst. Sol. 379 (2013) 7–11

[2] Hexweb, Honeycomb Attributes and Properties, 1999, Hexweb

[3] Roy, R., Park, S-J., Kweon, J-H., Choi, J-H., Characterization of Nomex honeycomb core constituent material mechanical properties, Composite Structures (2014), doi: http://dx.doi.org/10.1016/j.compstruct.2014.06.033

[4] M. Aegerter, N. Leventis, M. M. Koebel: Aerogels Handbook, Springer Verlag Heidelberg, (2011)

[5] http://building.dow.com/ap/en/apl/prop_styrofoam_lb.htm 4, last accessed 16.10.2014

[6] H. Maleki, L. Durães, A. Portugal, J. Non-Cryst. Sol. 385 55–74 (2014)

[7] J. H. Kim, C. M. Choi, S. R. Hwang, J. H. Kim, and Y. J. Oh, Korean J. Met. Mater. 48, 856 (2010).

[8] M. Schmidt and F. Schwertfeger J. Non-Cryst. Solids 225, 364 (1998).

[9] D. R. Ulrich, J. Non-Cryst. Solids 121, 465 (1990).

[10] J. Fricke and T. Tillotson, Thin Solid Films 297, 212 (1997).

[11] J. D. Mackenzie, J. Non-Cryst. Solids 100, 162 (1988).

[12] A. C. Pierre and G.M. Pajonk, Chem. Rev. 102, 4243 (2002).

[13] N. Hüsing, U. Schubert, Angew. Chem., 110, 22 - 47 (1998)

[14] http://www.dlr.de/wf/desktopdefault.aspx/tabid-9788/16788_read-40746/, last accessed 17.10.2014

[15] T. Enz, K. Heinrich, N. Hüsing, B. Milow, L. Ratke, G. Reichenauer, I. Smirnova, Sc, Summer School Aerogels 2010

[16] K. Sinkó, Materials 2010, 3, 704-740; doi:10.3390/ma3010704

[17] A.C. Pierre, History of Aerogels, in: Handbook on Aerogels, M.A. Aegerter, N. Leventis, M. Koebel, Springer Verlag Heidelberg, 2011, S. 9-18

[18] P.J. Davis, C. Jeffrey Brinker, D.M. Smith, J. Non-Cryst. Solids 142 189–196 (1992)

[19] L. Durães, M. Ochoa, N. Rocha, R. Patrício, N. Duarte, V. Redondo, et al., J. Nanosci. Nanotechnol. 12 6828–6834 (2012)

[20] J. P. Arenas, M. J. Crocker, MATERIALS REFERENCE ISSUE (2010)

[21] L.W. Hrubesh,J. Non-Cryst. Solids 225 (1998) 335 -342.

[22] J. L. Gurav, I. Jung, H. Park, E. S. Kang, D. Y. Nadargi, Journal of Nanomaterials Volume 2010, Article ID 409310

[23] A. C. Pierre, G. M. Pajonk, Chem. Rev. 102 (2002), 4243-4265

[24] G.M. Pajonk, Colloid Polym. Sci. (2003) 281: 637–651

[25] Y. K. Akimov, Instruments and Experimental Techniques, Vol. 46, No. 3 (2003)

[26] M. Schmidt, F. Schwertfeger, J. Non-Cryst. Sol. 225 (1998) 364–368

[27] R. A. Strøm, Y. Masmoudi, A. Rigacci , G. Petermann, L. Gullberg, B. Chevalier, M.-A. Einarsrud, J. Sol-Gel. Sci. Techn. (2007) 41:291–298.

[28] N. D. Hegde, A. Venkateswara Rao, J Mater Sci (2007) 42:6965–6971.

[29] A. Venkateswara Rao, S. D. Bhagat, Solid State Sciences 6 (2004) 945–952.

[30] A. Venkateswara Rao, G.M. Pajonk, S.D. Bhagat, P. Barboux, Journal of Non Crystalline Solids 350 (2004) 216–223.

[31] A. Karakoç, J. Freund, Composite Structures, 94 (2012) 2017–2024.

[32] http://www.hexcel.com/de/, last accessed on 24.10.2014.

[33] H. Junkers, DE310040 (1915)

[34] C. Dornier, GB515267, Dornier Metallbauten GmbH (1937)

[35] www.schuetz.net, last accessed on 28.07.2014.

[36] T. Bitzer, Honeycomb Technology: Materials, Design, Manufacturing, Applications and Testing, London 1997, Chapman & Hall.

[37] http://malekjafarian.com/?page_id=84, last accessed on 28.07.2014.

[38] http://www.schuetz.net/schuetz/SCH%C3%9CTZ%20Germany%20(HQ)/en/INDUSTRIAL%20SERVICES/CORMASTER/CORMASTER%20Honeycombs/CORMASTER%20C1/, last accessed on 25.6.2014.

[39] S. Hong, I. Song, Y. Park, H. Yun, K. Hwang Y. Rhee, Met. Mater. Int. 18, No. 3 (2012) 481-486.

[40] S. C. Joshi, Low velocity impact performance of aerogel-filled sandwich composites, ICCS 16 Porto, 2011

[41] M. Schwan, Novel superflexible resorcinol-formaldehyde aerogels and combining them with aramid honeycombs, in submission

[42] Prof. Dr. Ing. Hopmann, Vorlesungsskript Werkstoffkunde II, Institut für Kunststoffverarbeitung in Industrie und Handwerk an der RWTH Aachen; April 2013.

[43] D. Hull, T. W. Clyne, An introduction to composite materials, Cambride University Press 1996

[44] http://svfs.ifm.tu-berlin.de/mikromechanische_mischungsregeln.html#auto_top, last accessed on 19.7.2014.

[45] L. Ratke, M. Schestakow, B. Milow, J. Laskowski, M. Schwan, K. Ganesan, P. Niemeyer, A. K. Hajduk, I. Smirnova, P. Gurikow, M. Koebel, L. Huber, G. Reichenauer, N. Hüsing, European School on advanced aerogels, Deutsches Zentrum für Luft und Raumfahrt, Köln, 2012

[46] S.E. Gustafsson, Rev. Sci. Instrum, 62 (3) (1991) 797.

[47] Hot Disk AB, Hot DiskTM Manual Thermal Constants Analyser Model TPS 2500, Gothenburg (Sweden), 2006.

[48] http://www.c3-analysentechnik.de/hot-disk-messprinzip.php, last accessed on 06.9.2013.

[49] T. Log and S. E. Gustafsson, FIRE AND MATERIALS, 19 (1995) 43-49.

[50] G. E. Dieter, Mechanical metallurgy, New York 1986, 3rd edition, McGraw-Hill.

[51] Prof. Dr. Meyer, Vorlesungsskript Grundlagen der Rasterelektronenmikroskopie, Gemeinschaftslabor für Elektronenmikroskopie (GFE), RWTH Aachen 2012.

[52] G. I. Goldstein, D. E. Newbury, P. Echlin, D. C. Joy, C. Fiori, E. Lifshin, Scanning electron microscopy and x-ray microanalysis, New York 1981, Plenum Press.

[53] http://www.ammrf.org.au/myscope/images/sem/sem-ve-lm.png, last accessed on 23rd July 2014.

[54] S. Brunauer, P.H. Emmett, E. Teller, J. Am. Chem. Soc. 60 (1938) 309.

[55] K. S. W. Sing, D. H. Everett, R. A. W. Haul, L. Moscou, R. A. Pierotti, J. Rouqoerol, T.Siemieniewska, Pure & Applied Chemistry 57 (1985) 603-6019.

[56] E. P. Barrett et al., J. Am. Chem. Soc. 73 (1951) 373–380.

[57] P. Niemeyer, Synthesis & Properties of Flexible Silica Aerogels as a Precursor for Si-O-C Aerogels, Bachelor-Thesis, RWTH Aachen und Deutsches Zentrum für Luft und Raumfahrt, Köln, 2012

[58] P. R. Aravind, P. Niemeyer, L. Ratke, Microporous and Mesoporous Materials 181 (2013) 111–115.

[59] T. Bitzer, Honeycomb Technology - Materials, Design, Manufacturing, Applications and Testing, Hexcel Corporation Dublin, CA USA 1997, Chapman & Hall

[60] G. Gottstein, Physikalische Grundlagen der Materialkunde, Aachen 2007, Springer Verlag